Determination of the Threshold Stress Intensity Factor and Velocity of Delayed Hydride Cracking of Endplate Welds in CANDU Fuel Bundles with Different Design and Manufacturers

NWMO TR-2010-25 December 2010

G. K. Shek

Kinectrics Inc.

nwmo
NUCLEAR WASTE MANAGEMENT ORGANIZATION
SOCIÉTÉ DE GESTION DES DÉCHETS NUCLÉAIRES

Nuclear Waste Management Organization
22 St. Clair Avenue East, 6th Floor
Toronto, Ontario
M4T 2S3
Canada

Tel: 416-934-9814
Web: www.nwmo.ca

DETERMINATION OF THE THRESHOLD STRESS INTENSITY FACTOR AND VELOCITY OF DELAYED HYDRIDE CRACKING OF ENDPLATE WELDS IN CANDU FUEL BUNDLES WITH DIFFERENT DESIGN AND MANUFACTURERS

NWMO TR-2010-25

December 2010

G. K. Shek
Kinectrics Inc.

Disclaimer:

This report does not necessarily reflect the views or position of the Nuclear Waste Management Organization, its directors, officers, employees and agents (the “NWMO”) and unless otherwise specifically stated, is made available to the public by the NWMO for information only. The contents of this report reflect the views of the author(s) who are solely responsible for the text and its conclusions as well as the accuracy of any data used in its creation. The NWMO does not make any warranty, express or implied, or assume any legal liability or responsibility for the accuracy, completeness, or usefulness of any information disclosed, or represent that the use of any information would not infringe privately owned rights. Any reference to a specific commercial product, process or service by trade name, trademark, manufacturer, or otherwise, does not constitute or imply its endorsement, recommendation, or preference by NWMO.

ABSTRACT

Title: **Determination of the Threshold Stress Intensity Factor and Velocity of Delayed Hydride Cracking of Endplate Welds in CANDU Fuel Bundles with Different Design and Manufacturers**
Report No.: **NWMO TR-2010-25**
Author(s): G. K. Shek
Company: Kinectrics Inc.
Date: December 2010

Abstract

The threshold stress intensity factor (K_{IH}) and crack velocity of DHC in the endplate welds of three unirradiated fuel bundles were determined. The three bundles included a GE 28-element bundle, a GE 37-element bundle and a CAMECO 37-element bundle. The results are compared with those obtained from previous tests on the endplate welds of two GE 37-element fuel bundles. There were no large differences in K_{IH} values and DHC velocities among the endplate welds of the three fuel bundles tested in the current program. The endplate welds of the three bundles have higher K_{IH} and lower DHCV values than the welds of the GE 37-element bundles tested previously.

TABLE OF CONTENTS

Page

ABSTRACT v

1. INTRODUCTION 1

2. METHODOLOGY 1

2.1 FUEL BUNDLES 1
2.2 HYDRIDING OF ENDPLATE/ENDCAP WELDS 2
2.3 METALLOGRAPHIC EXAMINATION OF WELDS 4
2.4 DESIGN OF TEST SAMPLE 8
2.5 TEST APPARATUS 9
2.6 TEST PROCEDURE 10
2.7 TEST MATRIX 11

3. RESULTS OF DHC TESTS 11

3.1 GE 37-ELEMENT BUNDLE 14
3.2 GE 28-ELEMENT BUNDLE 26
3.3 CAMECO 37-ELEMENT BUNDLE 39
3.4 OTHER OBSERVATIONS 53

4. DISCUSSION 54

4.1 APPLIED BENDING STRESSES AND K_{IH} VALUES FOR DHC INITIATION 54
4.2 DHC VELOCITY 56

5. CONCLUSIONS 57

ACKNOWLEDGEMENTS 57

REFERENCES 58

LIST OF TABLES

Page

Table 1: Identification of Empty Fuel Bundles 1
Table 2: Hydrogen Concentration of Hydrided Endplate Welds 4
Table 3: Initial Test Matrix 11
Table 4: Type and Number of Tests Performed in Test Program 11
Table 5: Summary of DHC Tests on the Endplate Welds of the Three Empty Bundles 12
Table 6: Summary of Tests on Elements in Outer Ring in Shek and Wasiluk (2009) 13

LIST OF FIGURES

Page

Figure 1: The empty fuel bundle elements sprung out after being parted from the bundle 2
Figure 2: Diffusion anneal of endplate welds 3
Figure 3: Endplate weld of element # 1 of the GE 37-element bundle 5
Figure 4: Endplate weld of element # 1 of the GE 28-element bundle 6
Figure 5: Endplate weld of element # 3 of the CAMECO 37-element bundle 7
Figure 6: Test sample for the DHC test of the endplate weld from the GE 37-element bundle 8
Figure 7: Schematic of test apparatus showing the loading arrangement 9
Figure 8: Loading arrangement of DHC Test rigs 10
Figure 9: Record of K_{IH} and DHCV tests in Test 09-106 on element #2 the GE 37-element bundle; sample loaded on ID side of endplate 14
Figure 10: Fracture surfaces of sample in Test 09-106 on GE 37-element bundle 15
Figure 11: Dimensions of welds measured from fracture surfaces of sample in Test 09-106 on GE 37-element bundle 16
Figure 12: Record of K_{IH} and DHCV tests in Test 09-120 on element # 5 of the GE 37-element bundle; sample loaded on the ID side of endplate 17
Figure 13: Fracture surfaces of sample in Test 09-120 on GE 37-element bundle 18
Figure 14: Dimensions of welds measured from fracture surfaces in Test 09-120 19
Figure 15: Fracture surfaces of sample in Test 09-136 on GE 37-element bundle 20
Figure 16: Dimensions of welds measured from fracture surfaces in Test 09-136 21
Figure 17: Fracture surfaces of sample in Test 09-148 on GE 37-element bundle 22
Figure 18: Dimensions of welds measured from fracture surfaces in Test 09-148 23
Figure 19: Record of K_{IH} and DHCV tests in Test 09-124 of the GE 37-element bundle; sample was loaded on the OD side of the endplate 24
Figure 20: Fracture surfaces of sample in Test 09-124 on GE 37-element bundle in which the OD side was loaded under tension 25
Figure 21: Dimensions of welds measured from fracture surfaces in Test 09-124 26
Figure 22: Sample for Test 09-125 from the GE 28-element bundle 27
Figure 23: Record of K_{IH} test in Test 09-125 on element # 2 of the GE 28-element bundle; sample loaded on the ID side of the endplate 28
Figure 24: Fracture surfaces of sample in Test 09-125 on GE 28-element bundle 29
Figure 25: Dimensions of welds measured from fracture surfaces in Test 09-125 on GE 28-element bundle 30
Figure 26: Fracture surfaces of sample in Test 09-130 on GE 28-element bundle 31

Figure 27: Dimensions of welds measured from fracture surfaces in Test 09-130 on GE 28 element bundle....32
Figure 28: Fracture surfaces of sample in Test 09-144 on GE 28-element bundle....33
Figure 29: Dimensions of welds measured from fracture surfaces in Test 09-144 on GE 28-element bundle....34
Figure 30: Fracture surfaces of sample in Test 09-172 on GE 28-element bundle....35
Figure 31: Dimensions of welds measured from fracture surfaces in Test 09-172 on GE 28 element bundle....36
Figure 32: Record of K_{IH} and DHCV tests in Test 09-182 on element # 8 of the GE 28-element bundle; sample loaded on the OD side of the endplate....37
Figure 33: Fracture surfaces of sample in Test 09-182 on GE 28-element bundle in which the OD side was loaded under tension....38
Figure 34: Dimensions of welds measured from fracture surfaces in Test 09-182 on GE 28 element bundle....39
Figure 35: Sample for Test 09-135 from the CAMECO 37-element bundle....40
Figure 36: Records of Test 09-135 on element #3 of the CAMECO 37-element bundle....41
Figure 37: DHC crack shown in metallographic section about 1.7 mm from mid-section of weld of sample from Test 09-135....42
Figure 38: Metallographic section near centre of weld of sample from Test 09-135....43
Figure 39: Record of K_{IH} test in Test 09-186 on element #18 of the CAMECO 37-element bundle; sample loaded on ID side of endplate....44
Figure 40: A small crack with thin oxide was observed on the sample of Test 09-186....45
Figure 41: Dimensions of welds measured from fracture surfaces in Test 09-186 on CAMECO 37-element bundle....45
Figure 42: Three sets of potential drop leads were placed on the sample of some of the tests performed on CAMECO 37-element fuel bundle....46
Figure 43: Record of KIH and DHCV tests in Test 09-204 on element # 5 of the CAMECO 37-element bundle; sample loaded on the ID side of endplate....46
Figure 44: Fracture surfaces of sample in Test 09-204 of CAMECO 37-element bundle....47
Figure 45: Dimensions of welds measured from fracture surfaces in Test 09-204....48
Figure 46: Sample for Test 09_208 from the CAMECO 37-element bundle; Element 16 is at one of locations with the radial brace between the outer and intermediate rings....49
Figure 47: Record of K_{IH} test in Test 09-208 on element # 16 of the CAMECO 37-element bundle....50
Figure 48: Fracture surfaces of sample in Test 09_208 on CAMECO 37-element bundle....50
Figure 49: Dimensions of welds measured from fracture surfaces in 09_208....51
Figure 50: Record of K_{IH} test in Test 10-16 of the CAMECO 37-element bundle....52
Figure 51: Fracture surfaces of sample in Test 10-16 on CAMECO 37-element bundle....52
Figure 52: Dimensions of welds measured from fracture surfaces in Test 10-16....53
Figure 53: Deflection of sample in Test 09-135 (CAMECO bundle, DHC ring #6) at different loading stages....54
Figure 54: Comparison of applied bending stress for DHC initiation of endplate welds from different fuel bundles....55
Figure 55: Comparison of K_{IH} values of endplate welds from different fuel bundles....55
Figure 56: Comparison of DHCV at 150°C of endplate welds from different fuel bundles....56

1. INTRODUCTION

The susceptibility of CANDU spent fuel bundles endplate-to-endcap resistance welds (hereafter referred to as endplate welds) to Delayed Hydride Cracking (DHC) while in long term dry storage is being assessed. In order to establish whether DHC is operative at the endplate welds during dry storage, material properties such as the stress intensity factor (K_{IH}) for DHC initiation and delayed hydride crack velocity (DHCV) are required. A test apparatus, test procedure and stress analysis methodology were developed and used to determine the K_{IH} and DHCV of the endplate welds from two General Electric (GE) 37-element unirradiated fuel bundles in 2008 [1, 2]. A total of five endplate welds were tested at 130°C and 150°C and the K_{IH} values of four welds ranged from 7.6 to 8.3 MPa$\sqrt{m}$. The other sample had a K_{IH} value of 13.6 MPa$\sqrt{m}$. The higher measured K_{IH} value could be due to difference in notch geometry or incipient crack in the weld. DHCV at 150°C of the welds was found to increase after a heat-tinting cycle. DHCV ranged from 5.7×10^{-10} m/sec to 2.1×10^{-9} m/sec prior to the heat-tinting. The DHCV range increased to 1.3×10^{-9} m/sec to 5.5×10^{-9} m/sec after the heat-tinting.

The objective of the current experimental program is to expand the database on K_{IH} and DHCV by testing the endplate welds from another GE 37-element bundle as well as from a GE 28-element bundle and a CAMECO 37-element bundle to cover different bundle designs and manufacturers.

2. METHODOLOGY

The methodology developed and demonstrated by Shek and Wasiluk (2009) was followed in the DHC testing of the endplate welds in the current test program. A description of the methodology is provided below and any deviation from the previous test program (Shek and Wasiluk. 2009) will be highlighted.

2.1 FUEL BUNDLES

Three empty unirradiated fuel bundles without the fuel pellets inside the fuel elements were used in the current test program: one GE 28-element bundle, one GE 37-element bundle and one CAMECO 37-element bundle. A second CAMECO 37-element bundle was also purchased which was kept as a spare. These empty fuel bundles were made using standard manufacturing and welding processes. The bundles do not have serial number and they were identified using the designation shown in Table 1.

Table 1: Identification of Empty Fuel Bundles

Bundle Type	Designated Bundle Identification Number
GE 28-element	GE-1
GE 37-element	GE-2
CAMECO 37-element	CAMECO
CAMECO 37-element	Not assigned (Spare)

2.2 HYDRIDING OF ENDPLATE/ENDCAP WELDS

In order for DHC to occur, the welds must have sufficient hydrogen for hydrides to form at the flaw tip. The endplate welds of one end of the fuel bundles were hydrided to a target hydrogen concentration of 40 ppm by weight using the electrolytic hydriding/thermal diffusion method, similar to that used in previous test program (Shek and Wasiluk. 2009). In this hydriding procedure, a solid hydride layer was deposited electrolytically on the surfaces on one end of the bundle submerged in a 0.1 Molar sulphuric acid electrolyte. After electrolytic hydriding, a 75 mm long portion of the bundle was parted by wire electrical discharge machining from the three bundles (Figure 1). It was noted that the fuel elements in all three end portions sprung out after cutting, likely due to

Figure 1: The empty fuel bundle elements sprung out after being parted from the bundle

the presence of residual stresses in the endplate assembly. The three end portion of the bundles were placed in a large oven (Figure 2) and annealed at 266°C for 47 hours to diffuse the hydrogen from the surface hydride layer into the bulk of the component to obtain a target hydrogen concentration of 40 ppm. It was noted that the CAMECO bundle had a different oxide colour than the GE bundles after the diffusion anneal. A coupon was taken from the endplate weld of each bundle for hydrogen concentration measurements. The remnant of the hydride layer on the coupon was removed by pickling and grinding. The Terminal Solid Solubility for hydride dissolution (TSSD) temperature of each coupon was measured by differential scanning calorimetry. The coupons were then sent to Nu-Tech to measure the hydrogen concentration by

hot extraction inert gas fusion analysis using a LECO instrument. Results of the TSSD temperature and hydrogen measurements are shown in Table 2.

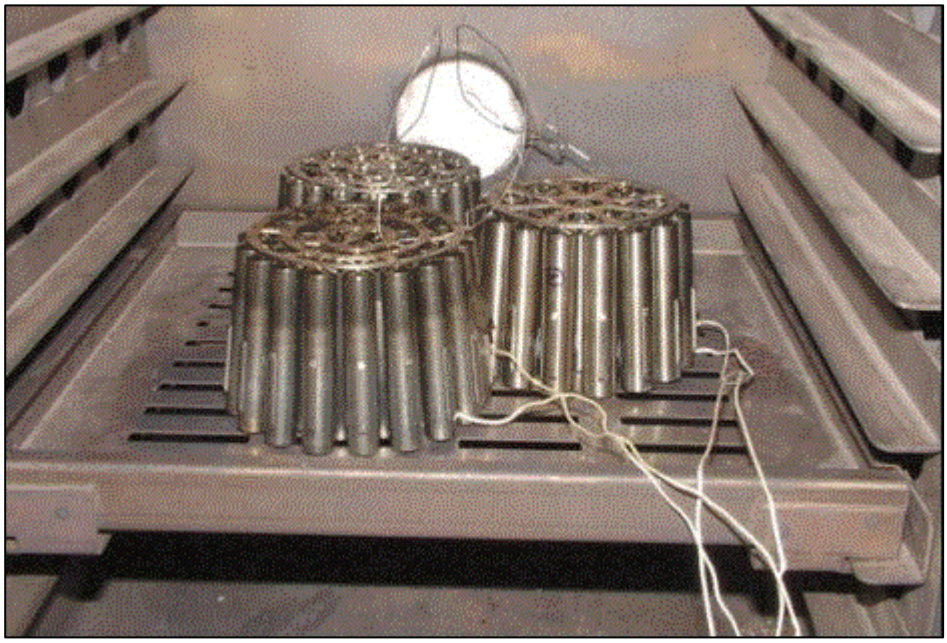

(a) End portion of the fuel bundles with surface hydride layer inside the oven for diffusion anneal

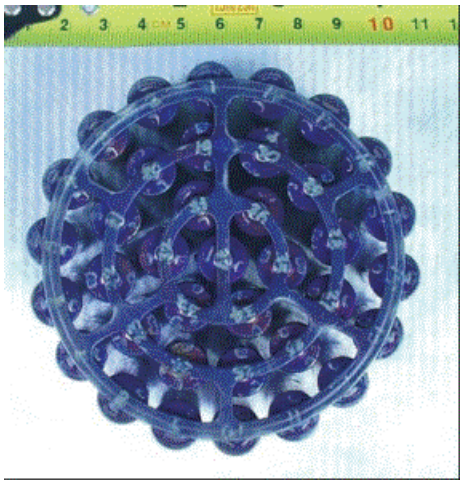

(b) Oxidized bundle after the diffusion anneal at 266°C for 47 hours

Figure 2: Diffusion anneal of endplate welds

Table 2: Hydrogen Concentration of Hydrided Endplate Welds

Fuel bundle type	Sample ID	TSSD Temperature (°C)	H concentration converted from Kearns TSSD equation[1] (ppm)	Measured hydrogen concentration by Nu-Tech (ppm)
GE 37-element	Hs9014	283	51	60.5
GE 28-element	Hs9015	285	52	54.9
CAMECO 37-element	Hs9016	288	55	59.0

[1]Kearns TSSD equation: TSSD (ppm) = 120000 exp(-35900/RT) [2]

The TSSD temperatures ranged from 283°C to 288°C, which are higher than the TSSD temperature of 270°C measured from the endplate weld of the hydrided bundle tested by Shek and Wasiluk (2009). Included in Table 2 are the converted hydrogen concentrations from the TSSD temperatures using Kearns TSSD equation on Zircaloy (Kearns. 1967). The converted hydrogen concentrations were lower than that determined by hot extraction analysis. The measured hydrogen concentrations ranged from 55-61 ppm which was higher than the targeted concentration of 40 ppm. This is acceptable as the DHC properties at the designed test temperature of 150°C would not be affected by the higher hydrogen concentration.

The remnant of the hydride layer was left on the bundles. This should have no impact on the DHC test results as the peak temperature in the DHC thermal cycle does not exceed the TSSD temperature of the hydrided samples so that there should not be additional hydrogen diffusion from the layer to the bulk during the DHC tests.

2.3 METALLOGRAPHIC EXAMINATION OF WELDS

One outer element endplate weld from each fuel bundle was prepared metallographically to examine the notch geometry between the endplate and endcap, and the weld discontinuity at the notch-tip which is the non-fused region of the resistance weld. The endplate weld was sectioned across the endplate in a slow-speed diamond wheel cutter near the edge of the weld, mounted and ground towards the centre of the weld. The section was polished with 9 µm diamond paste and a mirror-like surface finish was obtained by attack polishing in slurry of abrasive burnt ammonium dichromate ashes with the addition of a small amount of dilute hydrofluoric acid. The sample was then etched to show the weld region and heat-affected zone. The sample was examined under the optical microscope in the as-polished and etched conditions.

Figure 3 shows the cut section and the micrographs of the endplate weld from element #1 of the GE 37-element bundle at different magnifications. The elements are identified using the convention shown in Figure 2b (see also Figure 22 in later discussion). In Figure 3b, the OD

and ID side represents the outer diameter and inner diameter side of the outer ring of the endplate respectively. During manufacturing, a notch was formed between the endplate and the button-shape portion of the endcap. In this cross-section of the weld, it appears that the notch

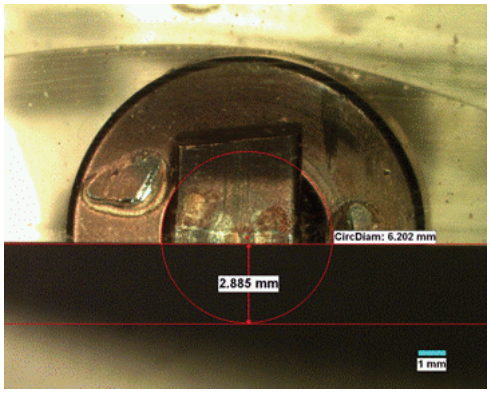

(a) Top view of sectioned endplate weld

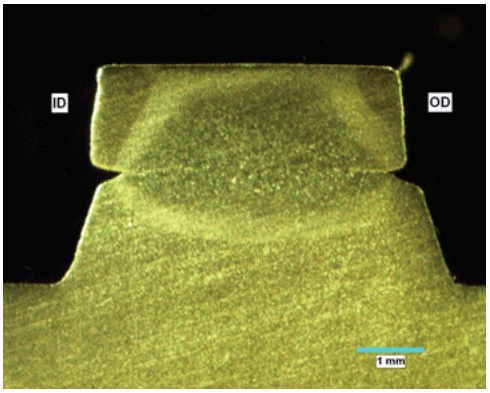

(b) Cross-section near centre of weld

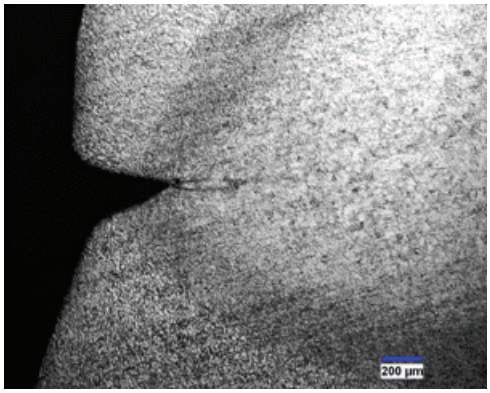

(c) Notch at ID side of weld

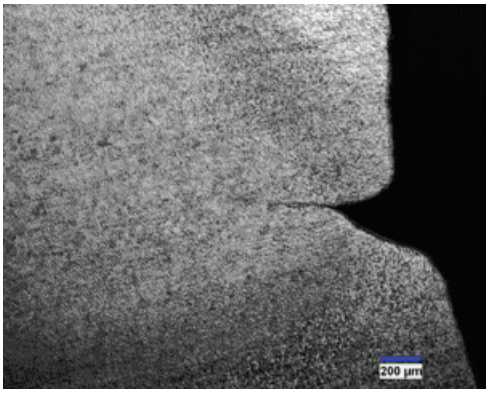

(d) Notch at OD side of weld

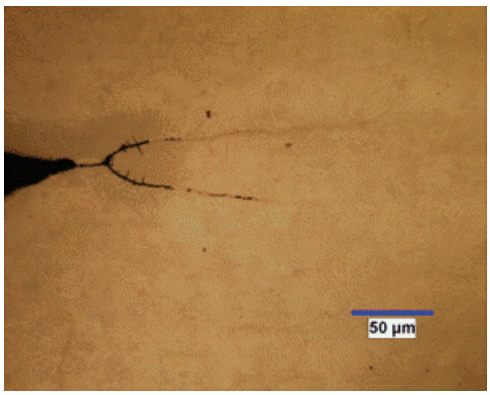

(e) Weld discontinuity at ID side

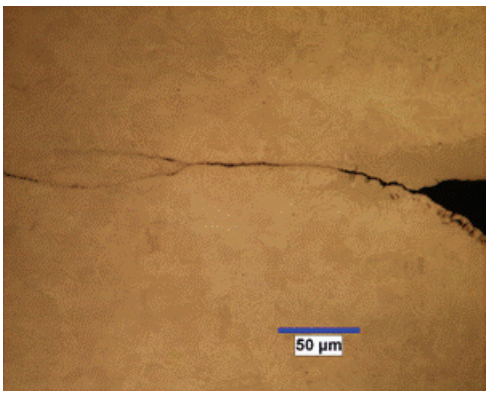

(f) Weld discontinuity at OD side

Figure 3: Endplate weld of element # 1 of the GE 37-element bundle

on the ID side was slightly deeper than that on the OD side (compare Figure 3c and 3d). A crack-like weld discontinuity was present at the notch tip. Overall, the notch geometry and weld discontinuity are similar to that observed in the endplate welds of the GE 37-element bundle tested by Shek and Wasiluk (2009).

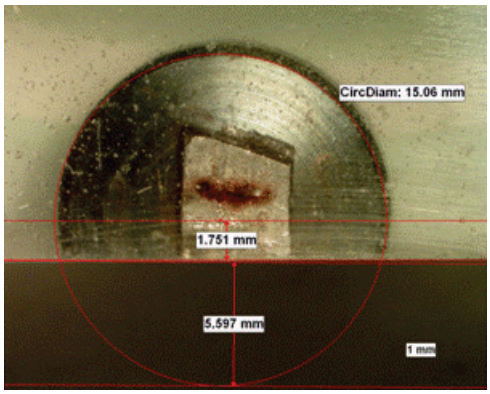

(a) Top view of sectioned endplate weld

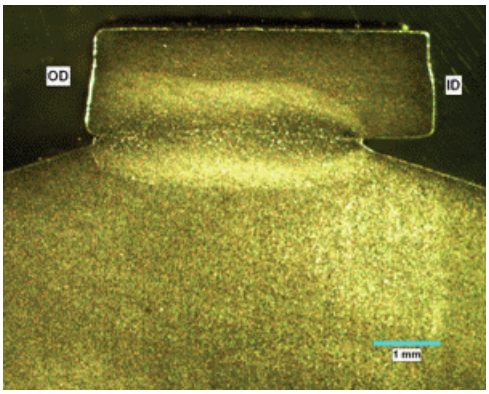

(b) Cross-section of weld

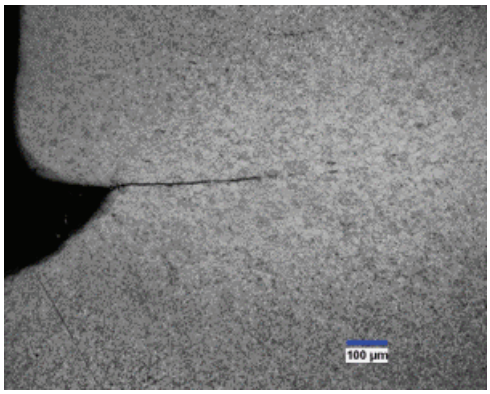

(c) Notch at OD side of weld

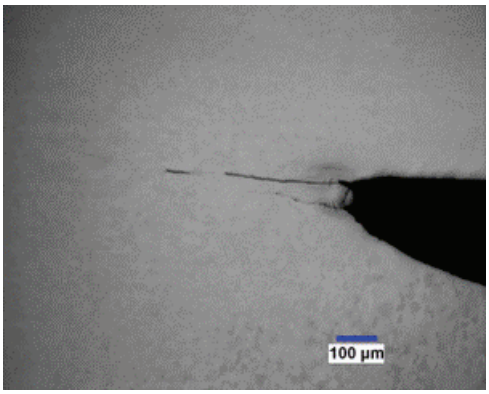

(d) Notch at ID side of weld

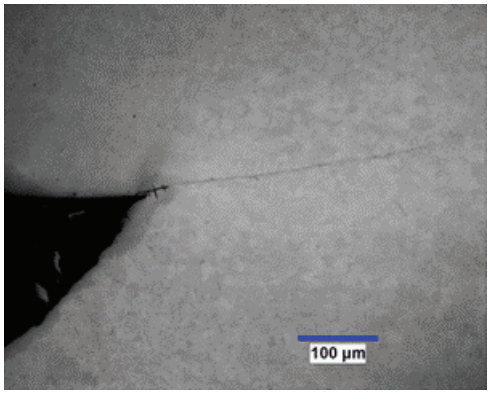

(e) Weld discontinuity at OD side

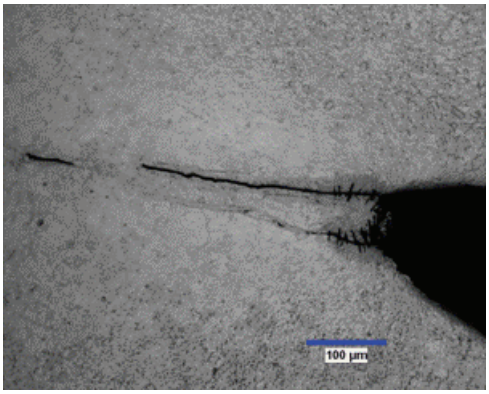

(f) Weld discontinuity at ID side

Figure 4: Endplate weld of element # 1 of the GE 28-element bundle

Figure 4 shows the metallographic section of the endplate weld of element #1 of the GE 28-element bundle. The endcap has a conical shape which is different than the button-shape endcap of the GE 37-element bundle. In this particular element, the weld was skewed towards the OD side of the endplate and therefore the notch depth on the OD side was a lot smaller than that on the ID side. The notch on the ID side of the GE 28-element bundle was deeper than that of the GE 37-element bundle welds. The notch radius and weld discontinuity appear to be similar to that of the GE 37-element bundle.

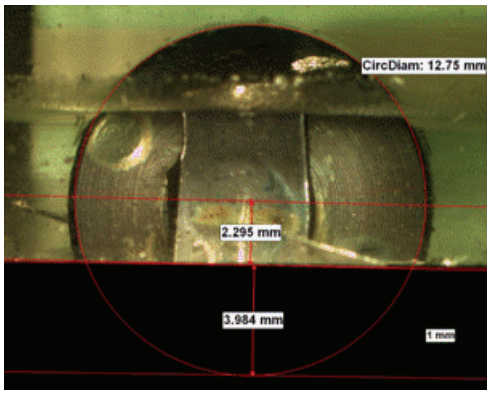

(a) Top view of sectioned endplate weld

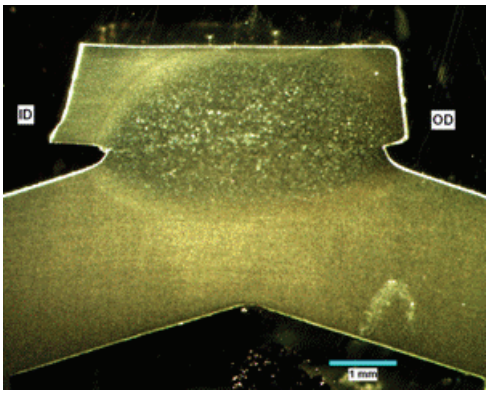

(b) Cross-section of weld

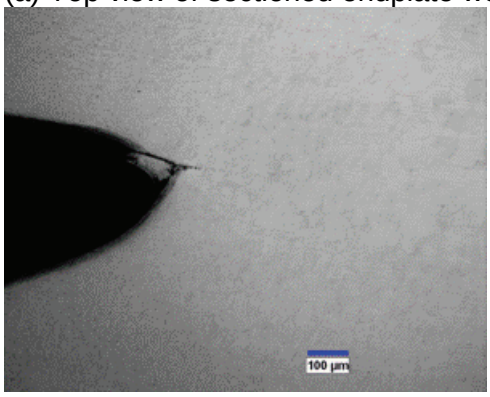

(c) Notch at ID side of weld

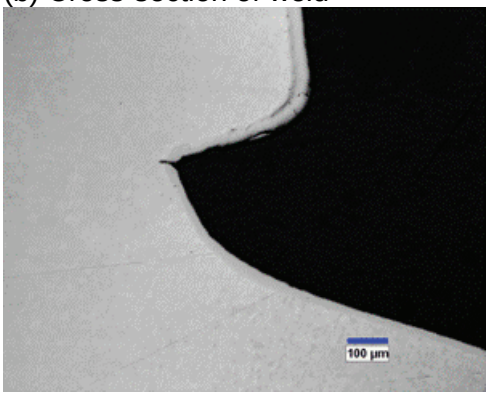

(d) Notch at OD side of weld

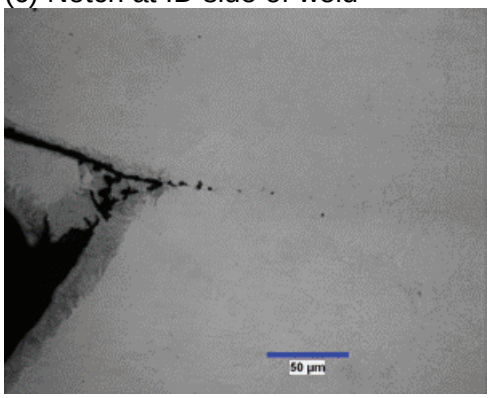

(e) Weld discontinuity at ID side

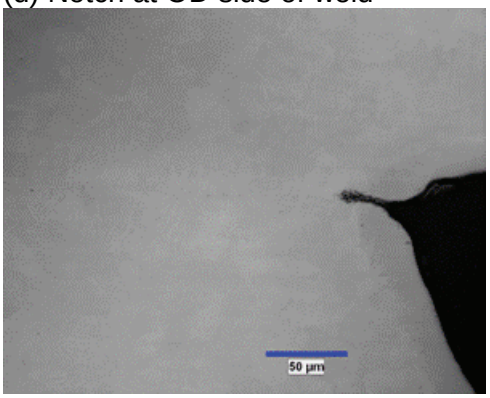

(f) Weld discontinuity at OD side

Figure 5: Endplate weld of element # 3 of the CAMECO 37-element bundle

Figure 5 shows the metallographic section of the endplate weld of element # 3 of the CAMECO 37-element bundle. In this particular element and cross-section, the weld was skewed towards the OD side of the endplate which reduced the notch depth. The endcap has a conical shape similar to that of the GE 28-element bundle. However, the notch radius appears to be blunter than that of the GE 37-element and 28-element bundles. In addition, the weld discontinuity was either non-existent or much smaller than that of the GE bundles. Overall, the endplate weld of the CAMECO bundle is larger in weld area than those of the GE bundles (see also Figure 38 in a later discussion).

In summary, there are differences in weld size, notch depth and profile, and weld discontinuity among the three types of fuel bundles. There are also differences in notch depth between the OD and ID side of the endplate weld. This will likely affect the applied load for DHC initiation as the stress concentration will be affected by the dimension of the notch and the depth of the weld discontinuity. However, this should not affect the K_{IH} value as it is a material property.

2.4 DESIGN OF TEST SAMPLE

Figure 6 shows the test sample which is similar to that used in previous tests (Shek and Wasiluk. 2009). The test sample is designed to have the weld region loaded in bending in a cantilever loading arrangement. It is noted that the endplate strip is slightly bent away from the fuel element as a result of the welding. As will be discussed in the next section, the sample is

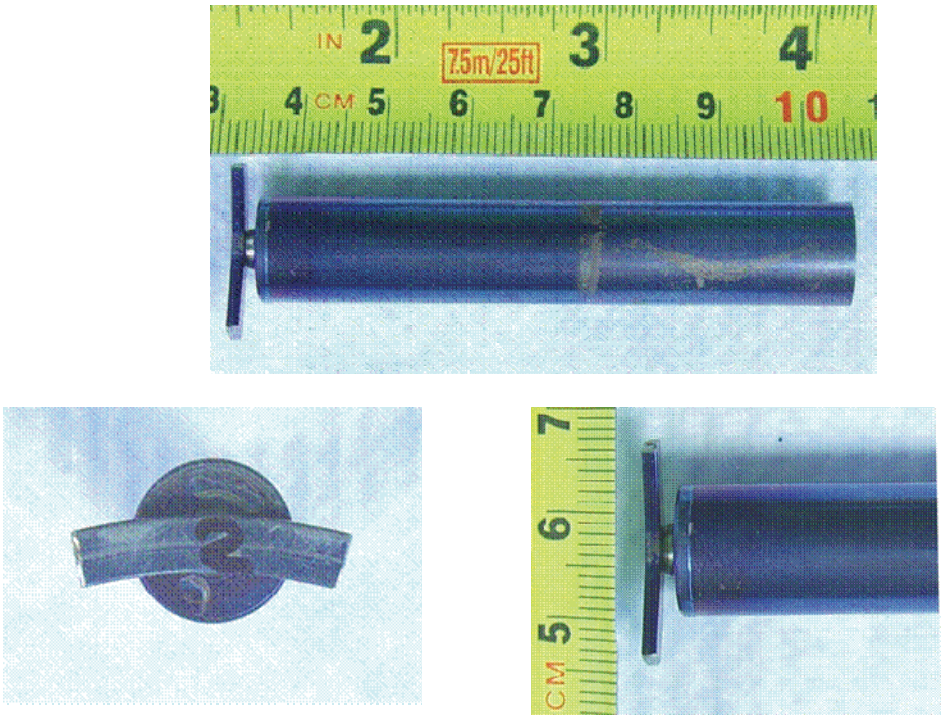

Figure 6: Test sample for the DHC test of the endplate weld from the GE 37-element bundle

anchored at the endplate strip and a bending stress is applied at the weld by pulling on the fuel element. The weld can be loaded under tensile bending stress either at the OD side or the ID side of the endplate. In Shek and Wasiluk (2009), all DHC tests were performed with the welds loaded on the ID side. A similar procedure was followed in the current K_{IH} tests. Both the bending stress and K_I for DHC initiation will be determined.

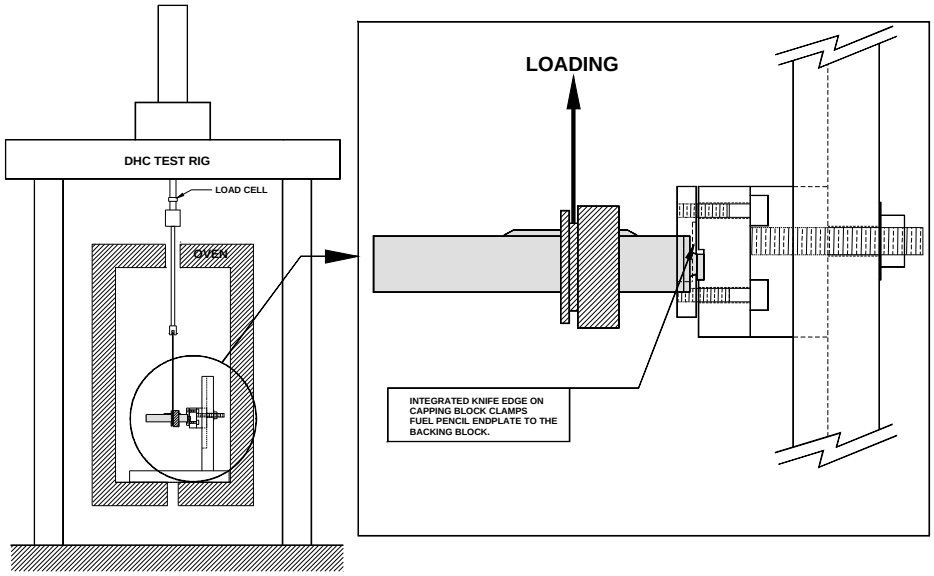

Figure 7: Schematic of test apparatus showing the loading arrangement

2.5 TEST APPARATUS

The tests were performed in two loading frames identified as DHC rig # 4 and DHC rig # 6. DHC rig #4 has been used in the previous test program (Shek and Wasiluk. 2009). Figure 7 shows a schematic diagram of the loading rig, sample holder and furnace for heating. As in Shek and Wasiluk (2009), the sample is anchored by gripping the endplate strip between two machined blocks. Details of the design of the loading blocks are given in Shek and Wasiluk (2009). In the current test program, the same loading blocks were used for the endplate welds of the GE 37-element fuel bundle. However for the endplate welds of the GE-28 element bundle and the CAMECO 37-element bundle, a new capping block was machined with a thinner extension as there was less clearance between the endplate and the endcap of these two bundles. The sample is loaded by pulling up on the fuel element through a steel cable placed around a groove in an aluminum collar attached to the fuel element. This produces a tensile bending stress in the lower part of the weld. The pull rod is connected to a load cell and an actuator, controlled by a stepper-motor. Figure 8(a) is a photograph showing the sample loaded in DHC rig # 4.

For DHC rig # 6, the actuator is located in the lower part of the screw-driven load frame. The load is applied by pulling the steel cable which exerts a tensile bending stress on the upper part of the weld. Figure 8(b) is a photograph showing the sample loaded in DHC rig # 6.

For both test rigs, heating is provided by a furnace with a programmable temperature controller. The allowable temperature fluctuation in the isothermal K_{IH} or DHCV tests is ± 2ºC from the target temperature. Crack initiation and growth is monitored by direct current potential drop technique. Acoustic emission is also used as a supplementary technique to detect cracking.

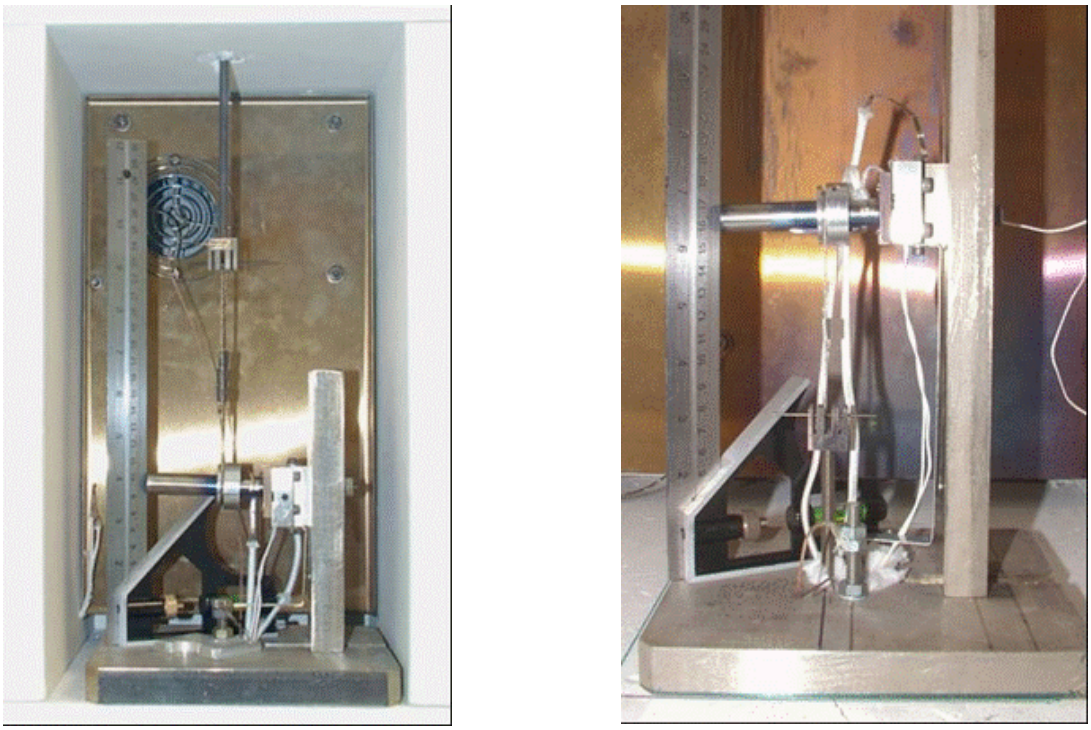

(a) DHC rig #4 (b) DHC rig #6

Figure 8: Loading arrangement of DHC Test rigs

However, it was shown to be ineffective in detecting cracking for this test material at 150°C (Shek and Wasiluk. 2009). The sample temperature, applied load, acoustic emission and potential drop voltages are monitored and recorded with a computerized data acquisition system.

2.6 TEST PROCEDURE

The test procedure is similar to that used in previous tests (Shek and Wasiluk. 2009). In order to save time and test material, the K_{IH} and DHCV tests are performed on the same test sample. Both tests are performed at 150°C. The K_{IH} test is performed first using the increasing load procedure as in Shek and Wasiluk (2009). In the increasing load test procedure, the applied load is increased in small steps at regular time interval until cracking is detected. In general, the sample is loaded to a load level below the estimated K_{IH} value, heated to a temperature of at least 220°C, held for an hour, and then cooled to 150ºC for cracking to occur. If no cracking is detected in about 50 hours, the applied load is increased by 5% and held for another 50 hours for cracking to initiate. The hold time in between load increase is to allow sufficient time for hydride growth at each load level. This process is repeated until cracking is detected.

After cracking has been detected, the load is maintained to obtain DHC crack growth for about 24 or more hours. A heat-tinting cycle is performed to mark the DHC crack from the K_{IH} test and then cooled to 150°C with a small load so that there is no crack extension during cooling. This completes the K_{IH} portion of the test. If DHCV test is required, the load is increased to about 1.3 times the K_{IH} load to continue DHC growth for about 50 hours. DHCV at 150°C is determined by the cracking time from the potential drop record and the maximum crack length measured from post-test examination of the fracture surface.

2.7 TEST MATRIX

The test matrix in the original proposal is shown in Table 3. It was planned to measure K_{IH} and DHCV at 150°C of five outer element endplate welds from each of the three fuel bundles. All samples will be loaded on the ID side of the endplate welds, similar to that of the previous tests (Shek and Wasiluk. 2009). However, the test matrix was later revised to cover testing both the ID and OD side of the endplate welds. In addition, the number of DHCV tests was reduced in order to cut down on the test time. Table 4 summarizes the type of tests actually performed on each bundle in this program.

Table 3: Initial Test Matrix

Bundle type	Test Temperature	# of K_{IH} test loaded on the ID side	# of DHCV test
GE 37-element	150°C	5	5
GE 28-element	150°C	5	5
CAMECO 37-element	150°C	5	5

Table 4: Type and Number of Tests Performed in Test Program

Bundle type	Test Temperature	# of K_{IH} test loaded on the ID side	# of K_{IH} test loaded on the OD side	# of DHCV test
GE 37-element	150°C	4	1	5
GE 28-element	150°C	4	1	4
CAMECO 37-element	150°C	4	1	1

3. RESULTS OF DHC TESTS

A complete K_{IH} test consists of three parts: (i) perform the increasing load test to determine the applied load for DHC initiation; (ii) post test examination of the DHC fracture surface and measure dimensions of endplate welds to determine the notch and initial crack depths and weld area; (iii) determine the K_{IH} value by finite-element analysis using the crack initiation load and endplate weld dimensions. A description of the finite-element methodology on the calculation of stress intensity factor for DHC initiation from the endplate welds is provided in Wasiluk (2011). Key experimental results are detailed below. A summary of the results from all three bundles is provided in Table 5.

Table 5: Summary of DHC Tests on the Endplate Welds of the Three Empty Bundles

Test #	Bundle type	Element #	DHC rig	Tensile stress on ID or OD side	DHC initiation load (N)	Bending stress for DHC initiation (MPa)	K_{IH} (MPa√m)	DHCV at 150°C prior to heat tinting (m/sec)	DHCV at 150°C after heat tinting (m/sec)	Postulated location for DHC initiation based on fracture surface examination
09-106	GE 37-element	2	4	ID	64	282	11.2	6.12 E-10	1.33 E-9	~45° from top
09-120	GE 37-element	5	6	ID	63	282	10.7	4.46 E-10	1.54 E-9	~45° from top
09-136	GE 37-element	8	4	ID	72	334	11.1	5.01 E-10	1.56 E-9	~45° from top
09-148	GE 37-element	15	4	ID	76	367	13.1	8.57 E-10	2.93 E-9	~45° from top
09-124	GE 37-element	17	4	OD	83	346	12.2	1.23 E-9	2.31 E-9	~45° from top
09-125	GE 28-element	2	6	ID	53	227	10.1	1.29 E-9	NA	Top of weld
09-130	GE 28-element	4	6	ID	53	214	10.0	1.45 E-9	2.55 E-9	Top of weld
09-144	GE 28-element	15	6	ID	56	220	13.6	1.41E-9	3.26 E-9	Top of weld
09-172	GE 28-element	6	6	ID	53	225	9.4	1.20 E-9	5.05 E-9	Top of weld
09-182	GE 28-element	8	6	OD	67	285	11.6	4.46 E-10	2.17 E-9	~45° from top
09-135	CAMECO	6	6	ID	73*	253	NA	NA	NA	~45° from top
09-186	CAMECO	18	4	ID	85	277	12.2	NA	NA	~45° from top
09-204	CAMECO	5	4	ID	80	255	12.1	8.41 E-10	1.78 E-9	~45° from top
09-208	CAMECO	16	6	ID	80	325	NA	7.0 E-10	NA	~45° from top
10-16	CAMECO	9	4	ID	93*	324	13.5	NA	NA	~45° from top

*****based on estimated cracking time; NA: Not Available

Table 6: Summary of Tests on Elements in Outer Ring in Shek and Wasiluk (2009)

Test ID	Type of Test	H conc. (ppm)	Test Temp. (°C)	Maximum nominal bending stress at crack initiation (MPa)	K_I for DHCV test or K_{IH} (MPa√m)	DHCV (m/sec)		Postulated location for DHC initiation based on fracture surface examination
						Before heat-tinting	After heat-ting	
07_09	K_{IH} test	10	130	184	8.3	4.7E-10	5.4E-10	Top of weld
07_67	K_{IH} test	40	150	163	7.7	2.5E-10	NA	Top of weld
07_104	K_{IH} test	40	150	167	7.9	6.8E-10	2.3E-09	Top of weld
07_140	K_{IH} test	40	150	170	7.6	2.1E-10	4.0E-10	Not clear
07_164	K_{IH} test	40	150	155	13.6	6.6E-10	2.1E-9	Top of weld
07_78	DHCV	40	150	214	11.8	2.1E-9	4.0E-9	Top of weld
07_79	DHCV	40	150	209	12.2	1.8E-9	5.5E-9	Top of weld

3.1 GE 37-ELEMENT BUNDLE

For the GE 37-element bundle, five K_{IH} tests were performed with four samples loaded on the ID side and one sample loaded on the OD side of the weld. In addition, DHCV tests were performed after the K_{IH} tests on all five samples. Details of the tests are provided below and the results are summarized in Table 5.

Test 09-106: This test was performed on the endplate weld of element #2 in DHC rig # 4 with the ID side of the endplate loaded under tension. The sample was subjected to both the K_{IH} and DHCV test procedures. Figure 9 shows the records of load, temperature, potential drop and acoustic emission of Test 09-106. The sample was loaded to about 43 N and then heated to 240°C, cooled and held at 150°C.

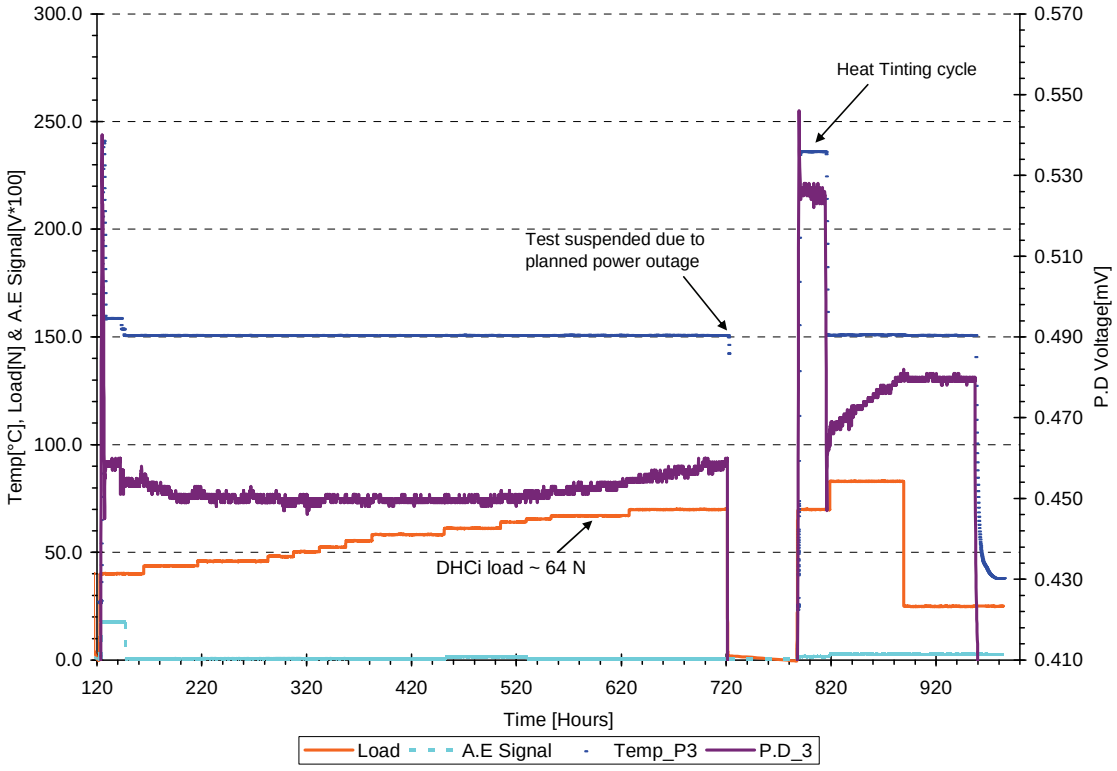

Figure 9: Record of K_{IH} and DHCV tests in Test 09-106 on element #2 the GE 37-element bundle; sample loaded on ID side of endplate

The load was increased incrementally at regular time intervals. The potential drop started to increase when the load was increased to 64 N. This was taken to be the crack initiation load. As observed in Shek and Wasiluk (2009), the acoustic emission technique was ineffective in detecting hydride cracking. The K_{IH} test was terminated after about 213 hours of crack growth

in which the load was raised to a final level of 70 N to obtain a steady crack growth, prior to a scheduled power outage. After the power outage, the DHC test was re-started by loading to 70 N and heated to 236°C, held for about 20 hours to heat-tint the DHC fracture surface. During the heat-tinting period, there was no increase in DHC growth as the temperature was approached by heating, similar to that observed in Shek and Wasiluk (2009). The temperature was then lowered to 150°C and the load was increased to 83 N for the DHCV portion of test. Cracking re-initiated without incubation time, as indicated by the steady increase in potential drop. The DHC test was terminated after 73 hours of crack growth.

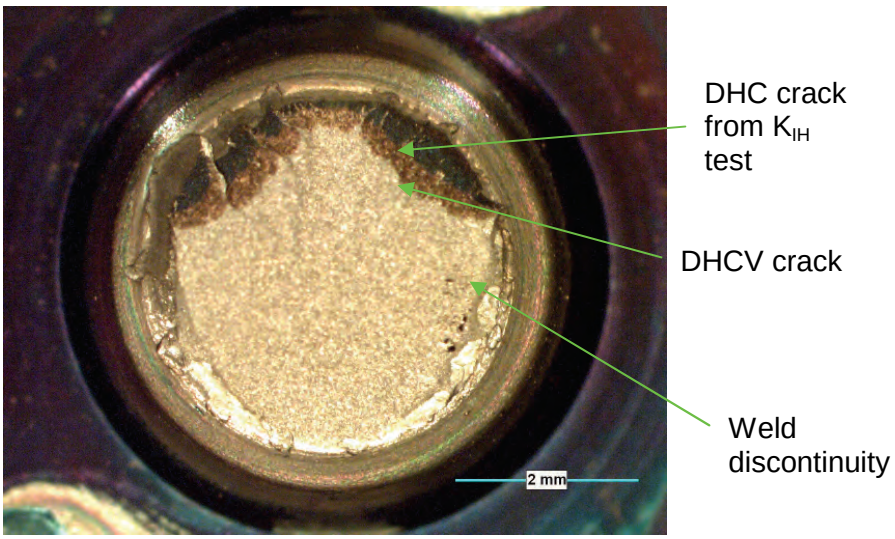

(a) Fracture surface on endcap side

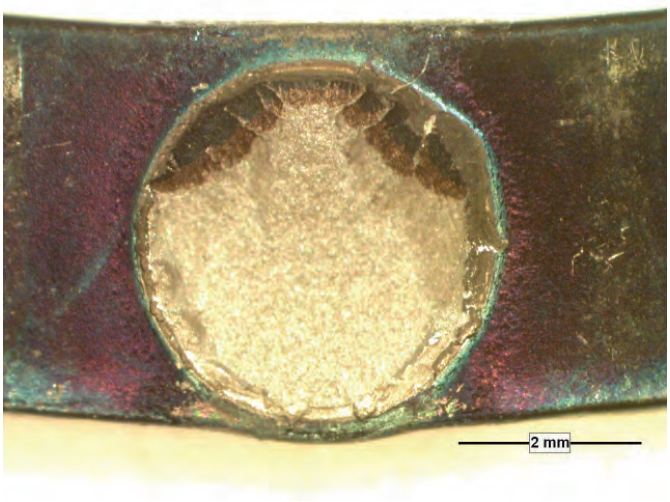

(b) Fracture surface on endplate side

Figure 10: Fracture surfaces of sample in Test 09-106 on GE 37-element bundle

The sample was broken open to reveal the DHC fracture surface. Figure 10a shows the fracture surfaces on the endplate and endcap sides. The two segments of DHC cracks corresponding to the K_{IH} and DHCV tests can be observed clearly, as well as the weld continuity. The first crack segment with the darker oxide occurred during the K_{IH} test. This crack segment did not have uniform depth around the perimeter of the weld and was longer at the two locations about 45° deviated from the top of the weld. This non-uniform crack shape indicates that the stress field at the endplate weld can be quite complex and cracking may not have initiated at the top of the weld.

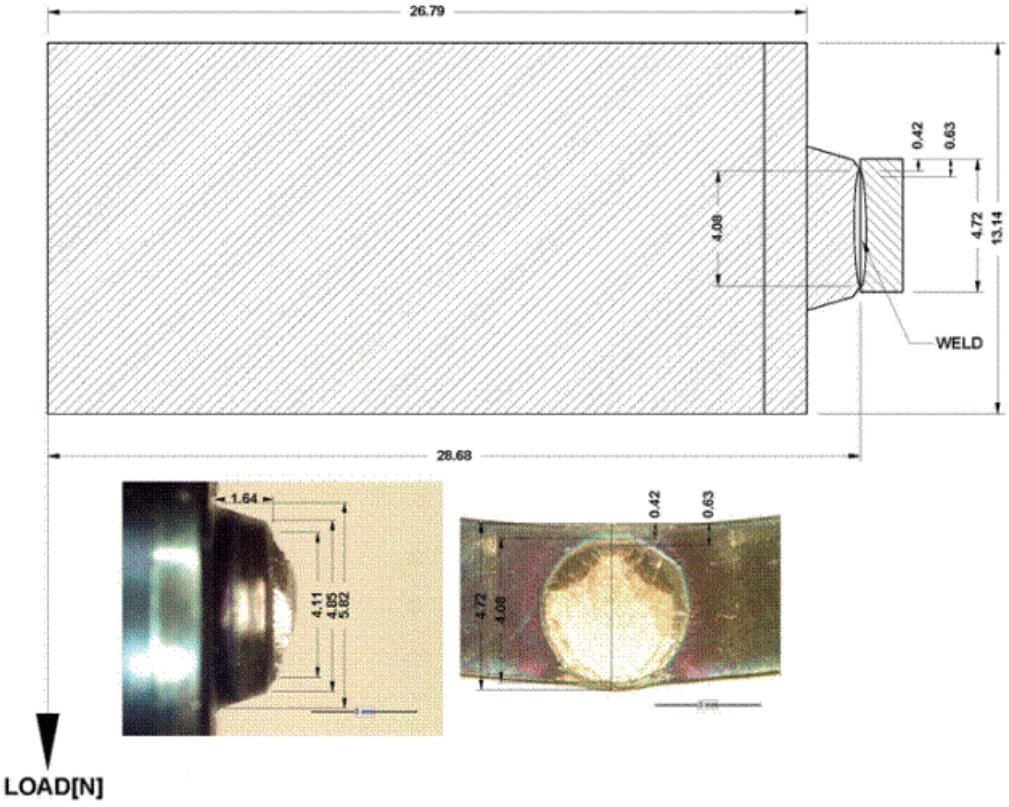

Figure 11: Dimensions of welds measured from fracture surfaces of sample in Test 09-106 on GE 37-element bundle

Figure 11 shows the various dimensions measured from the fracture surfaces of the welds on the endplate and endcap side, as well as a schematic diagram of the endplate and endcap notch constructed from the measured dimensions. In this weld, the notch depth on the ID side was determined to be 0.42 mm and the weld discontinuity was about 0.21 mm deep at the top of the weld.

Results of the K_{IH} and DHCV tests are summarized in Table 5, which lists the test number, bundle type, element identification number, loading orientation, applied load for DHC initiation, calculated bending stress for DHC initiation, K_{IH} values determined by finite-element stress

analysis, DHCV from the K_{IH} crack segment and after the heat-tinting, and the apparent location of crack initiation. Details on the calculation of bending stress and K_{IH} values are given in a separate report (Wasiluk. 2011)

Test 09-120: This test was performed on the endplate weld of element # 5 in DHC rig # 6, with the ID side of the endplate loaded under tension. Both K_{IH} and DHCV tests were performed and the results are summarized in Table 5. The test records are shown in Figure 12.

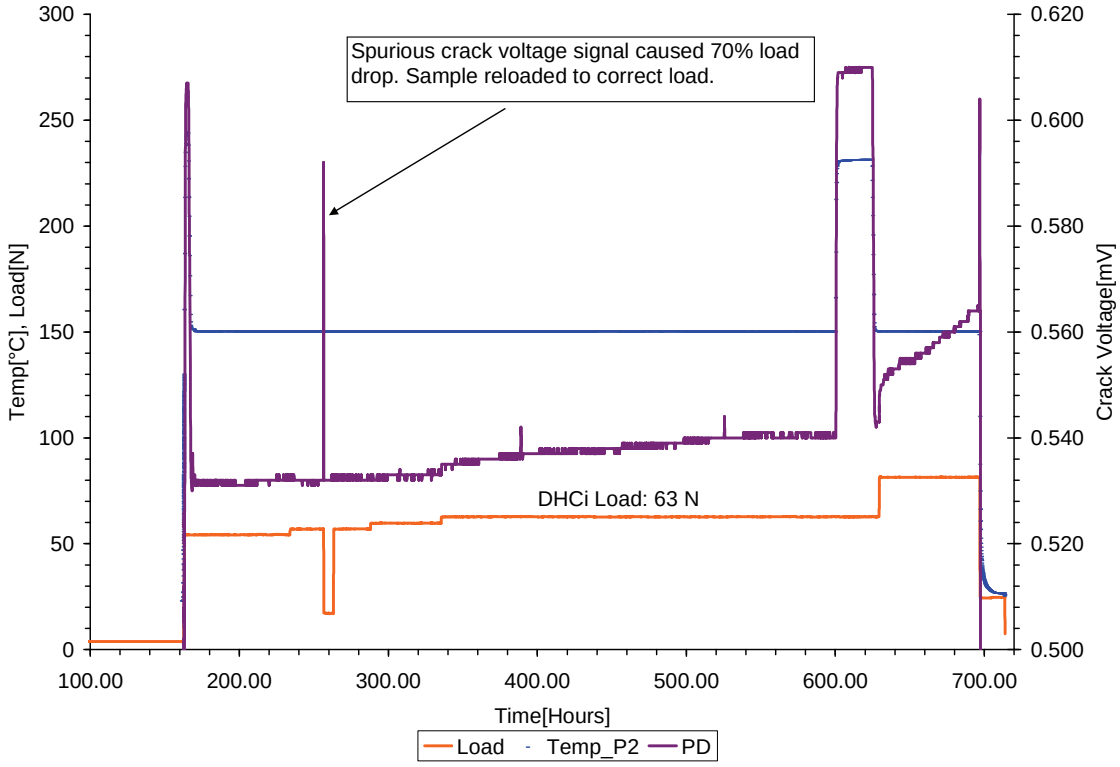

Figure 12: Record of K_{IH} and DHCV tests in Test 09-120 on element # 5 of the GE 37-element bundle; sample loaded on the ID side of endplate

There were spurious spikes in the d.c. potential drop during the test. A large spike occurred during the early part of the K_{IH} test which triggered a load-reduction. The load was restored to the same level prior to the load-reduction and testing was continued. Cracking was detected at an applied load of 63 N. This load was maintained for the remainder of the K_{IH} test. A couple of small voltage spikes occurred during this period after cracking has been initiated. The sample was then subjected to the heat-tinting cycle, followed by the DHCV test. It is judged that the spurious voltage spikes did not affect the test results, as they occurred either at a load level significantly below the crack initiation load or occurred after cracking has already been initiated.

Figure 13 shows the fracture surfaces of the DHC cracks on the endcap and endplate side. The two crack segments corresponding to the K_{IH} and DHCV are similar in appearance as that of Test 09-106. Cracking appeared to be initiated at the two locations about 45° from the top of the weld. Figure 14 shows the dimensions of the weld measured from the fracture surfaces and a schematic diagram of the endplate and endcap notch constructed from the measured dimensions.

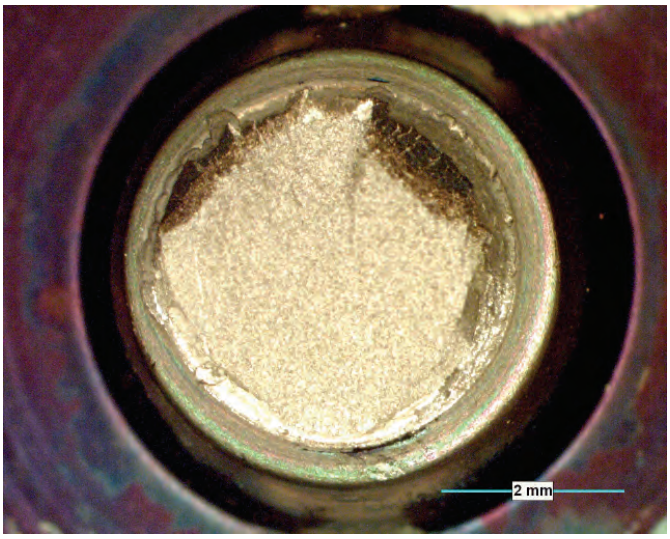

(a) Fracture surface on endcap side

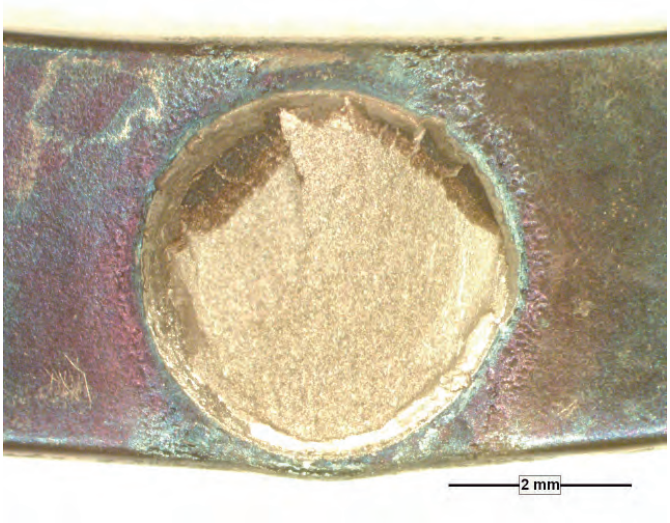

(b) Fracture surface on endplate side

Figure 13: Fracture surfaces of sample in Test 09-120 on GE 37-element bundle

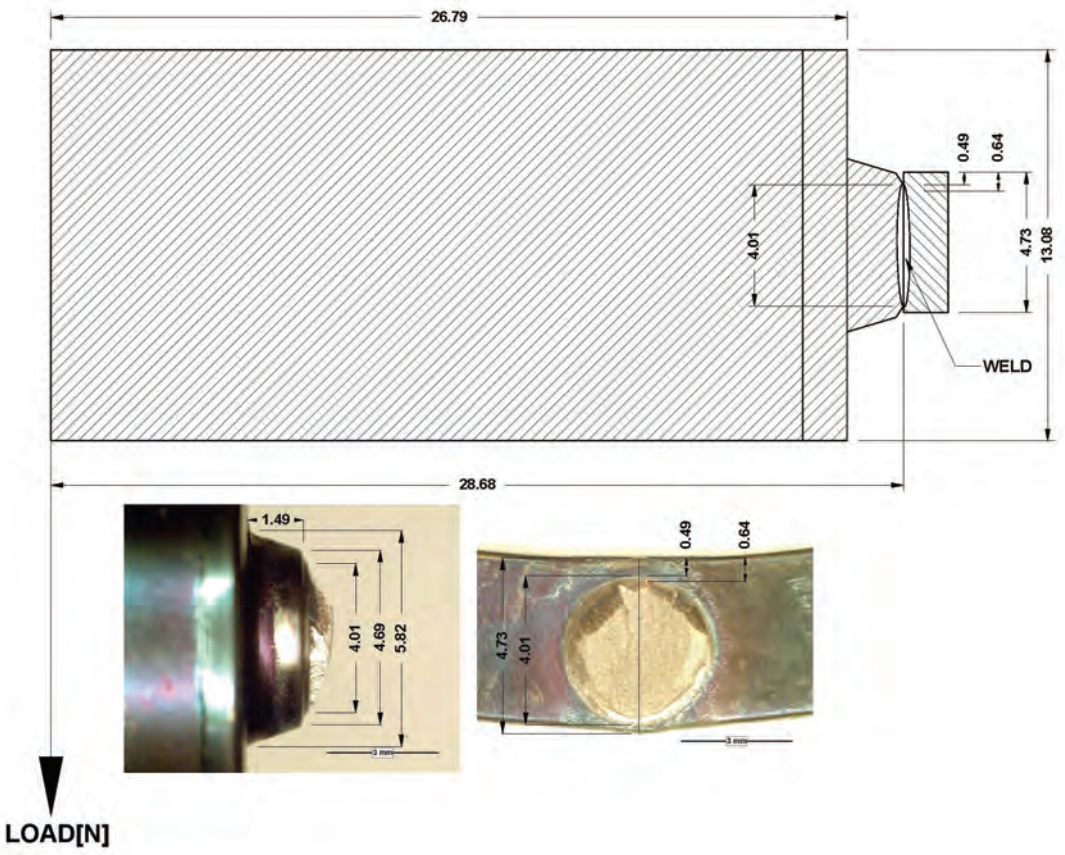

Figure 14: Dimensions of welds measured from fracture surfaces in Test 09-120

Test 09-136: This test was performed on the endplate weld of element # 8 in DHC rig # 4 with the ID side of the endplate loaded under tension. This sample was subjected to both the K_{IH} and DHCV test procedures. The test record was similar to that of Test 09-106. Crack initiation occurred at an applied load of 72 N.

Figure 15 shows the fracture surfaces of the DHC cracks on the endcap and endplate side. The endplate strip was torn off in the attempt to break open the cracked sample. The two crack segments corresponding to the K_{IH} and DHCV are clearly visible and cracking appeared to be initiated at the two locations about 45° from the top of the weld. Figure 16 shows the dimensions of the weld measured from the fracture surfaces and a schematic diagram of the endplate and endcap notch constructed from the measured dimensions.

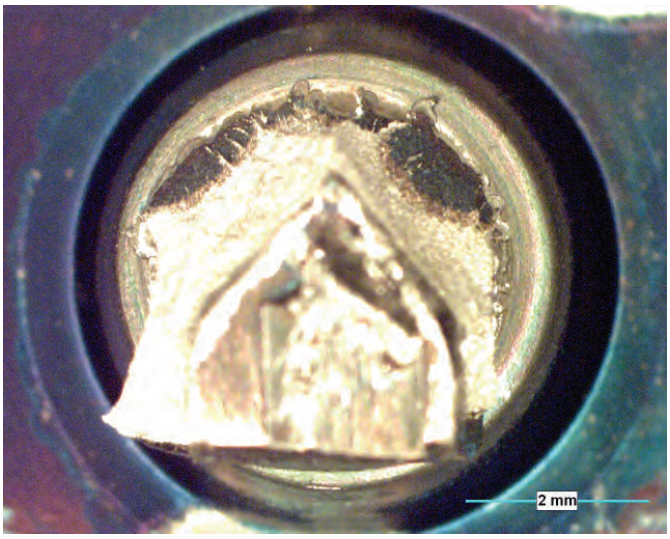

(a) Fracture surface on endcap side

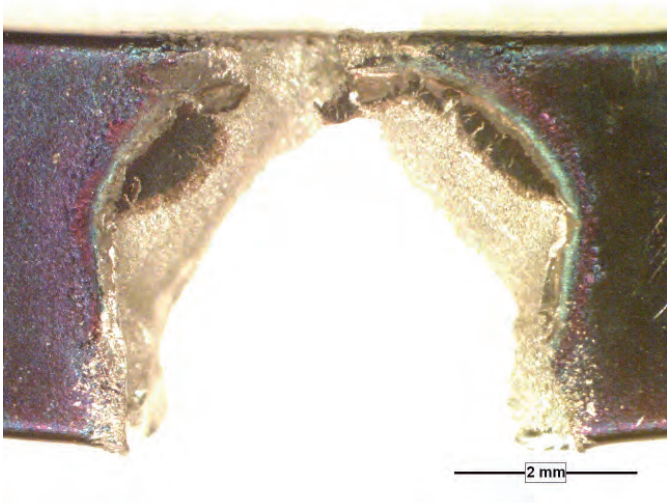

(b) Fracture surface on endplate side (endplate strip was torn)

Figure 15: Fracture surfaces of sample in Test 09-136 on GE 37-element bundle

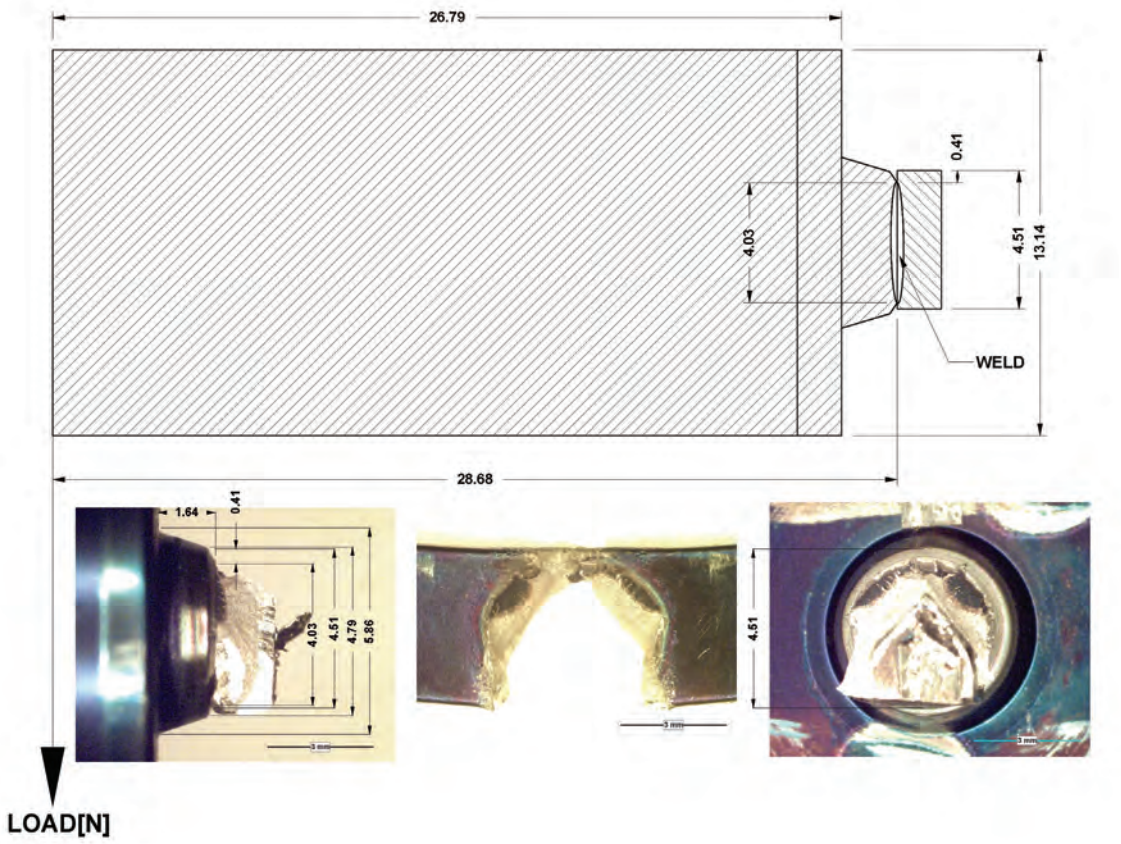

Figure 16: Dimensions of welds measured from fracture surfaces in Test 09-136

Test 09-148: This test was performed on the endplate weld of Element # 15 in DHC rig # 4 in which the ID side of the endplate weld was loaded under tension. This sample was subjected to both the K_{IH} and DHCV test procedures. The test record was similar to that of Test 09-106. Crack initiation occurred at an applied load of 76 N.

Figure 17 shows the fracture surfaces of the DHC cracks on the endcap and endplate side. The two crack segments corresponding to the K_{IH} and DHCV are clearly visible in which cracking appeared to be initiated at the two locations about 45° from the top of the weld. Figure 18

shows the dimensions of the weld measured from the fracture surfaces and a schematic diagram of the endplate and endcap notch constructed from the measured dimensions.

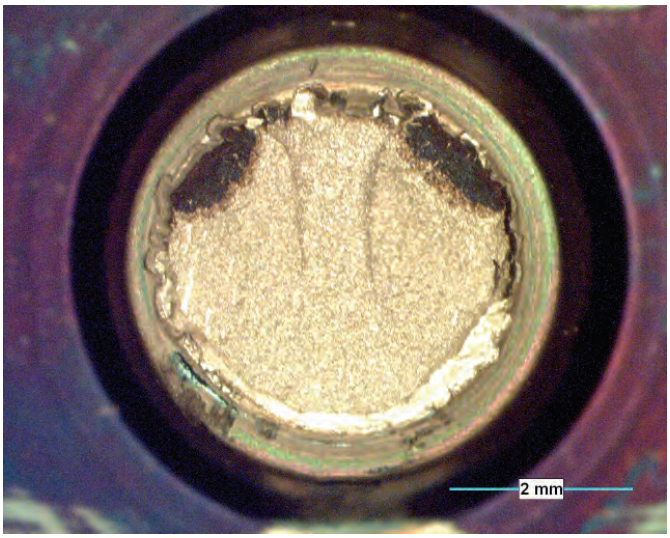

(a) Fracture surface on endcap side

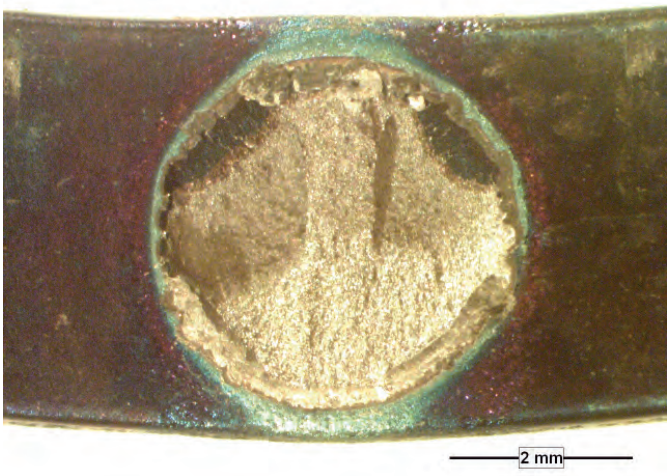

(b) Fracture surface on endplate side

Figure 17: Fracture surfaces of sample in Test 09-148 on GE 37-element bundle

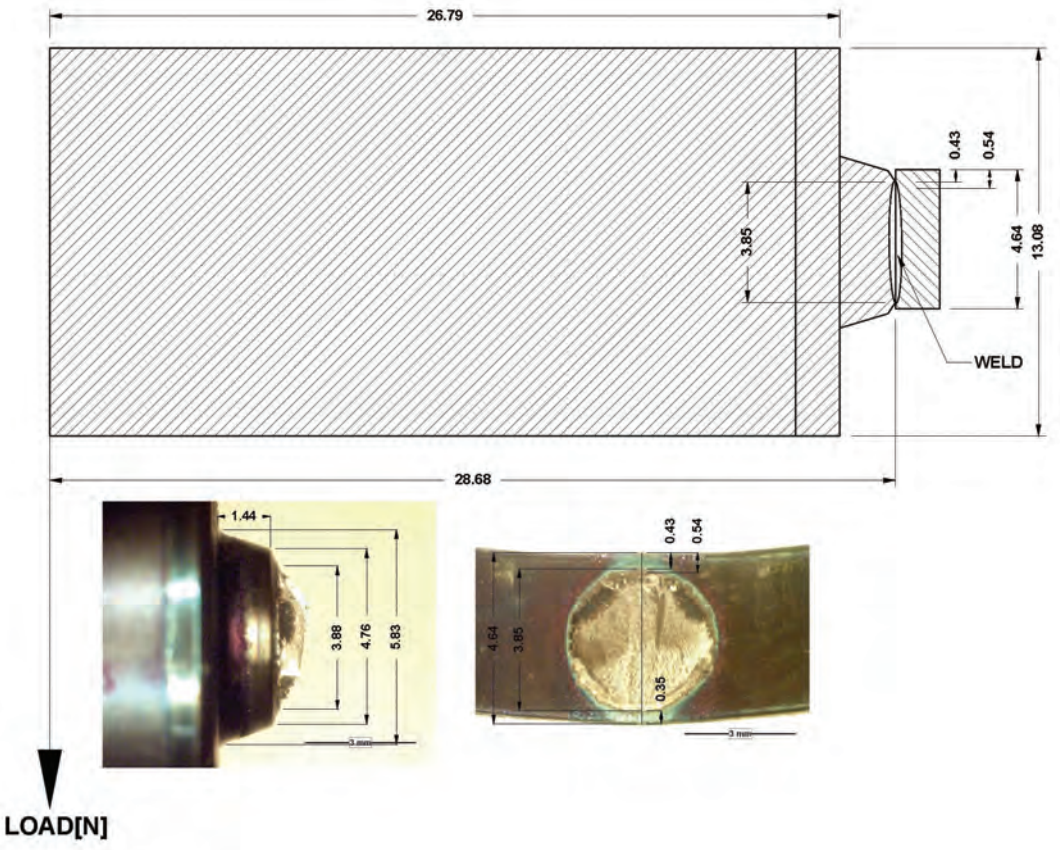

Figure 18: Dimensions of welds measured from fracture surfaces in Test 09-148

Test 09-124: : This test was performed on the endplate weld of Element # 17 in DHC rig # 4 with the OD side of the endplate loaded under tension. The sample was subjected to both the K_{IH} and DHCV test procedures. Figure 19 shows the test record which indicated that cracking initiated at an applied load of 83 N.

Figure 20 shows the fracture surfaces of the DHC cracks on the endcap and endplate side. The endplate strip was torn off in the attempt to break open the cracked sample. The two crack segments corresponding to the K_{IH} and DHCV are clearly visible in which cracking appeared to

be initiated at the two locations about 45° from the top of the weld. Figure 21 shows the dimensions of the weld measured from the fracture surfaces and a schematic diagram of the endplate and endcap notch constructed from the measured dimensions.

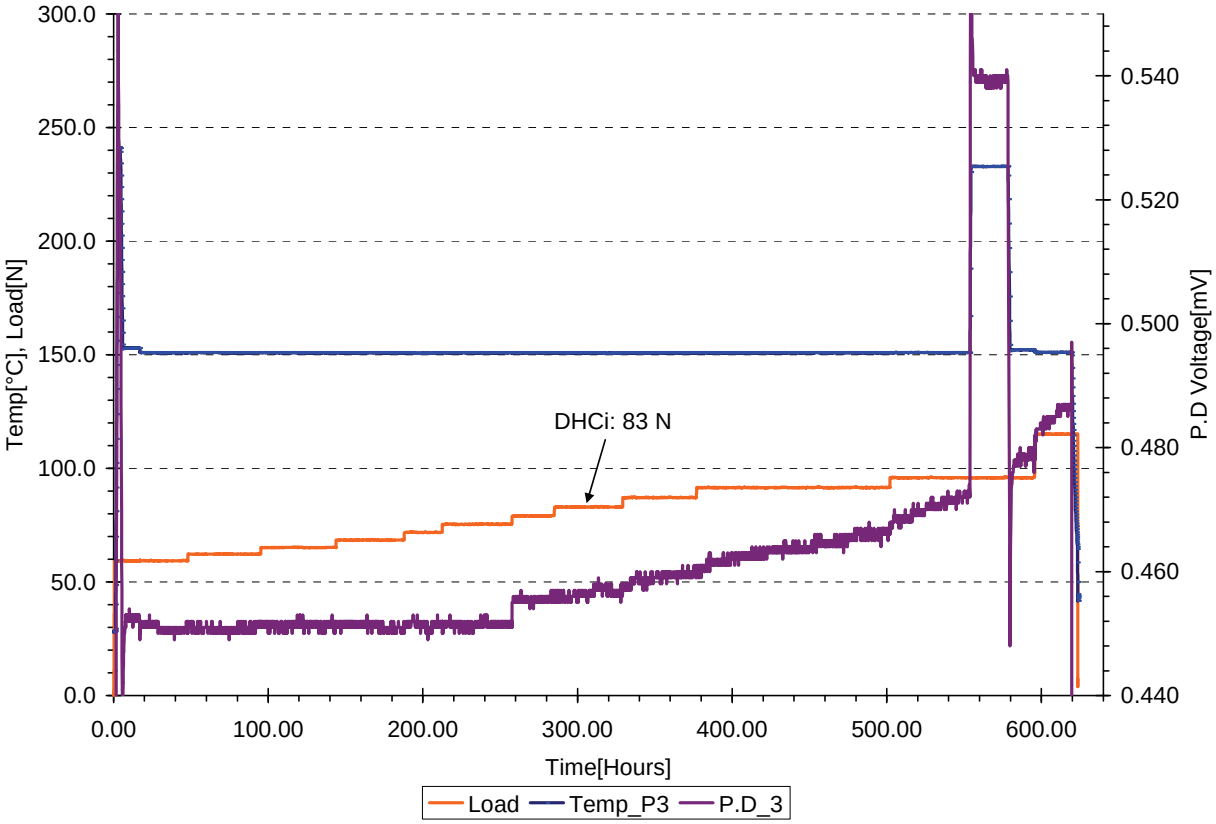

Figure 19: Record of K_{IH} and DHCV tests in Test 09-124 of the GE 37-element bundle; sample was loaded on the OD side of the endplate

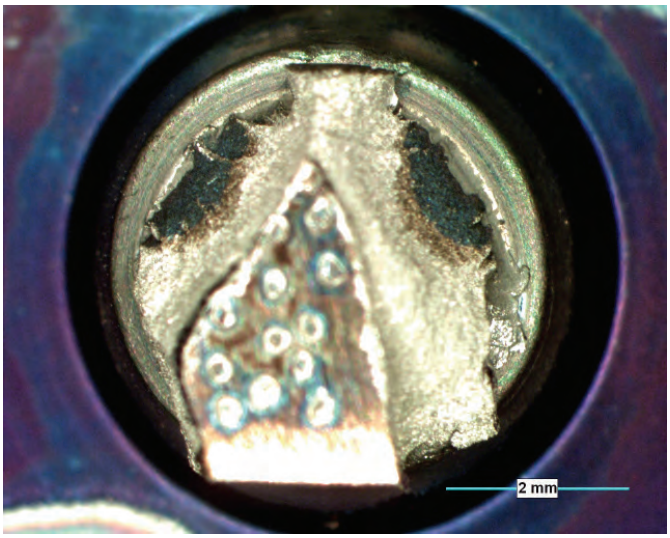

(a) Fracture surface on endcap side

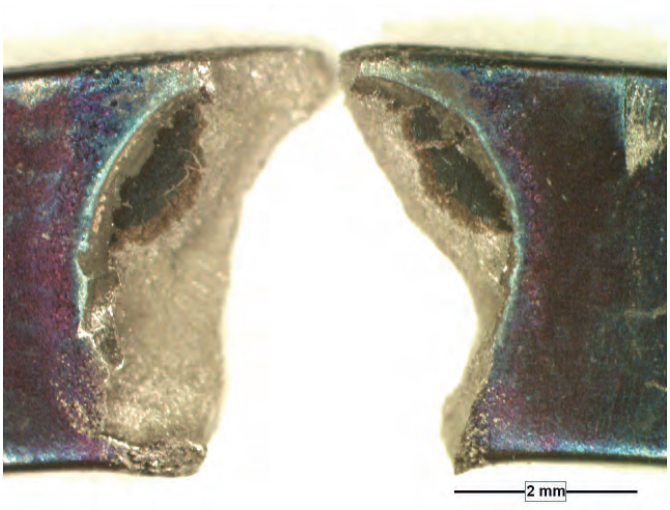

(b) Fracture surface on endplate side (strip was torn)

Figure 20: Fracture surfaces of sample in Test 09-124 on GE 37-element bundle in which the OD side was loaded under tension

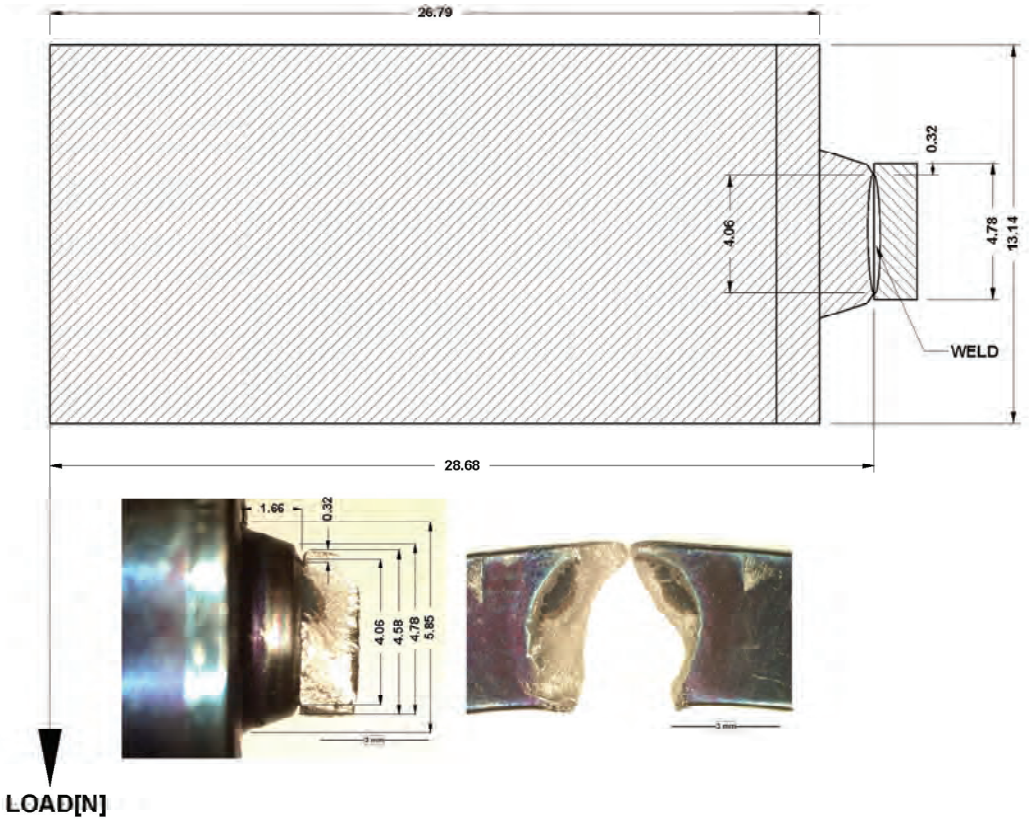

Figure 21: Dimensions of welds measured from fracture surfaces in Test 09-124

3.2 GE 28-ELEMENT BUNDLE

For the GE 28-element bundle, five K_{IH} tests were performed with four samples loaded on the ID side and one sample loaded on the OD side. In addition, DHCV tests were performed on four samples loaded on ID side after the K_{IH} tests. Details of the tests are provided below and the results are summarized in Table 5.

Test 09-125: This test was performed on the endplate weld of element # 2 in DHC rig # 6 with the ID side of the endplate loaded under tension. Figure 22 shows the test sample which was

subjected to the K_{IH} test only. Figure 23 shows the test record which indicated that cracking initiated at an applied load of 53 N and steady crack growth was obtained with further increase in load. The crack initiation load of 53 N is lower than that of the welds from the GE 37-element bundle.

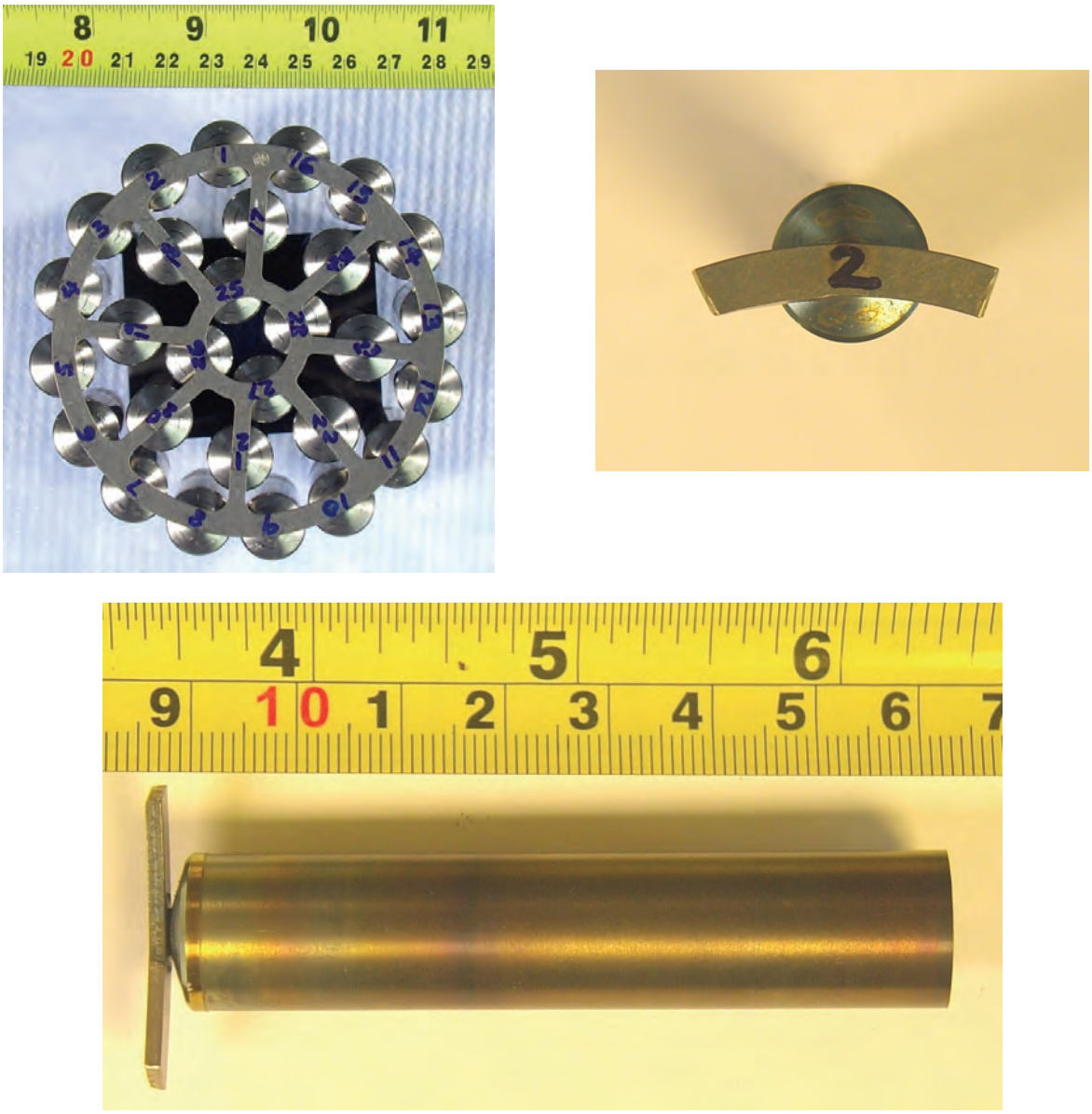

Figure 22: Sample for Test 09-125 from the GE 28-element bundle

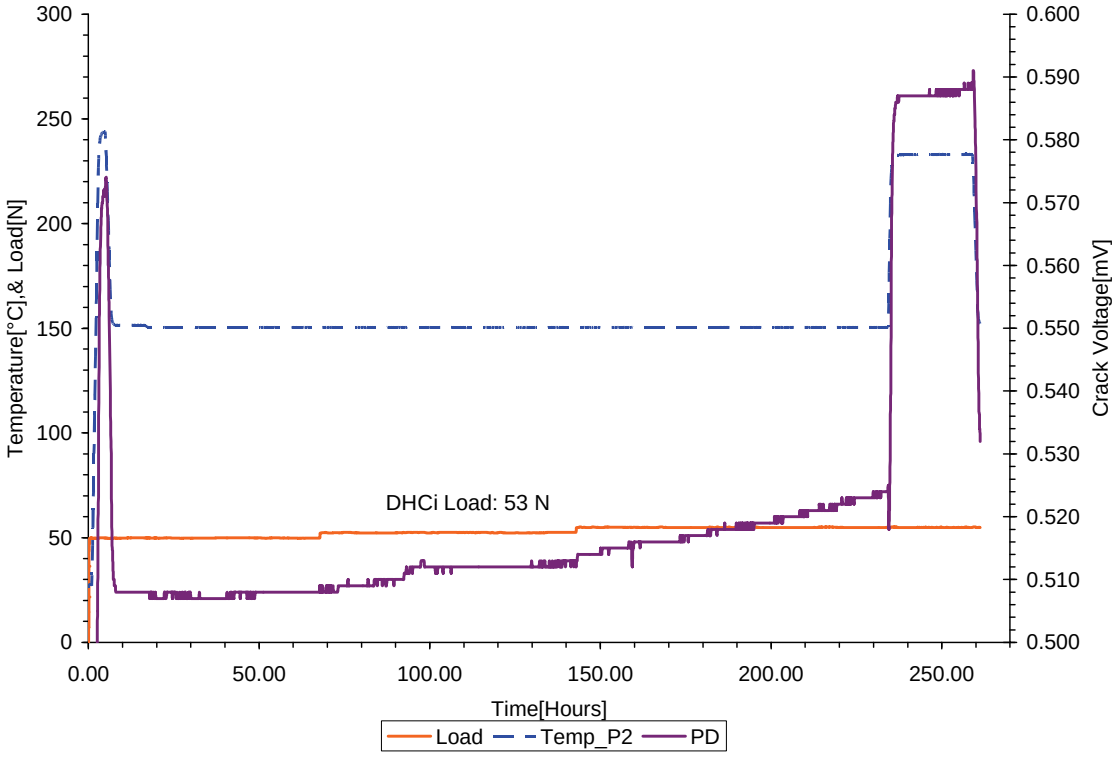

Figure 23: Record of K_{IH} test in Test 09-125 on element # 2 of the GE 28-element bundle; sample loaded on the ID side of the endplate

Figure 24 shows the fracture surface of the DHC crack after heat-tinting. The location of crack initiation appeared to be at the top of the weld, as the crack was longest at that location. The weld was skewed towards the OD side of the endplate. This is consistent with the result of metallographic examination shown in Figure 4. In addition, the weld area appeared to be closer to an elliptical shape instead of the “circular” shape observed in the welds of the GE 37-element bundle. Figure 25 shows the dimensions of the weld measured from the fracture surfaces and a schematic diagram of the endplate and endcap notch constructed from the measured dimensions. The notch depth on the ID side was deeper than that of the welds from the GE 37-element bundle, as a result of the weld skewing towards the OD side of the endplate. Therefore, it is expected that higher load will be required to initiate DHC from the OD side of the endplate.

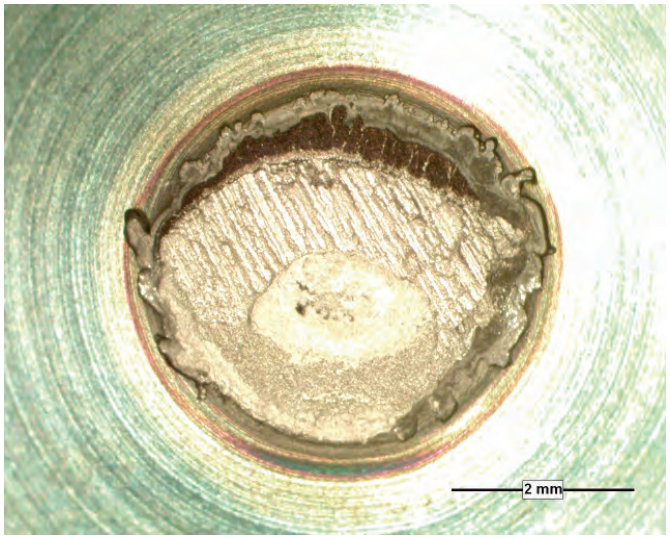

(a) Fracture surface on endcap side

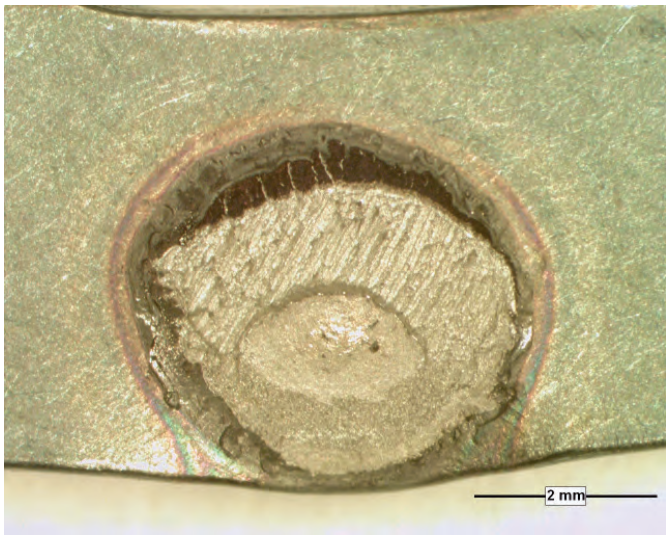

(b) Fracture surface on endplate side

Figure 24: Fracture surfaces of sample in Test 09-125 on GE 28-element bundle

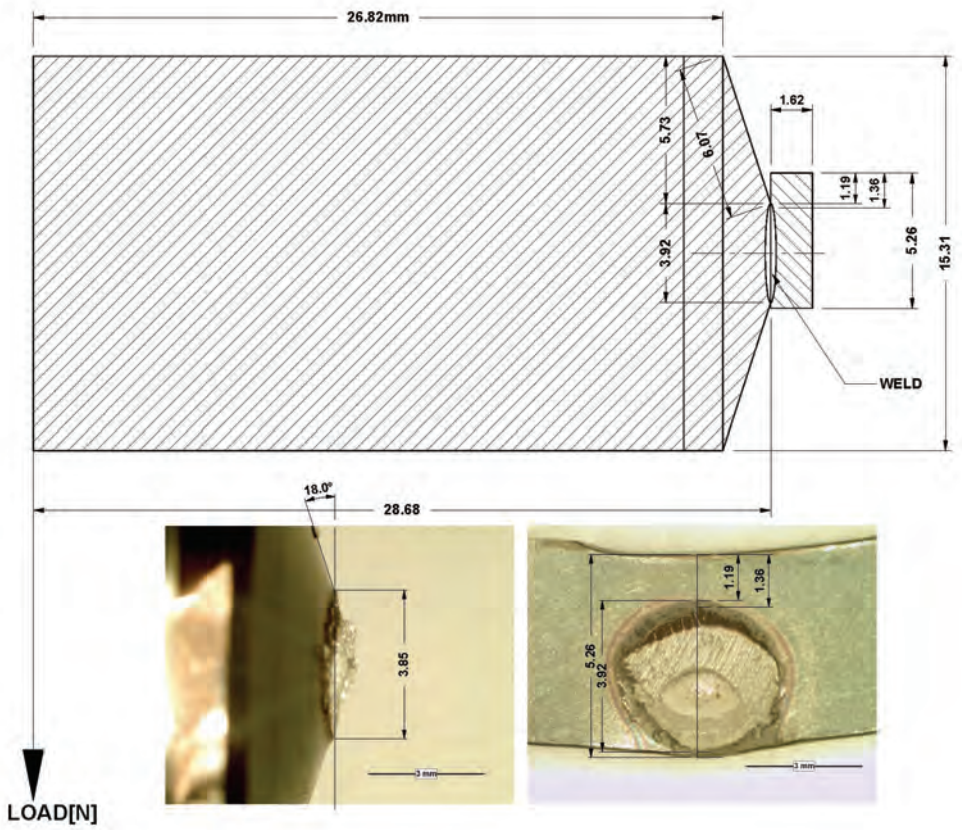

Figure 25: Dimensions of welds measured from fracture surfaces in Test 09-125 on GE 28-element bundle

Test 09-130: This test was performed on the endplate weld of element # 4 in DHC rig # 6 with the ID side of the endplate loaded under tension. The sample was subjected to both the K_{IH} and DHCV test procedure. The test record was similar to that of Test 09-124, and cracking was initiated at an applied load of 53 N.

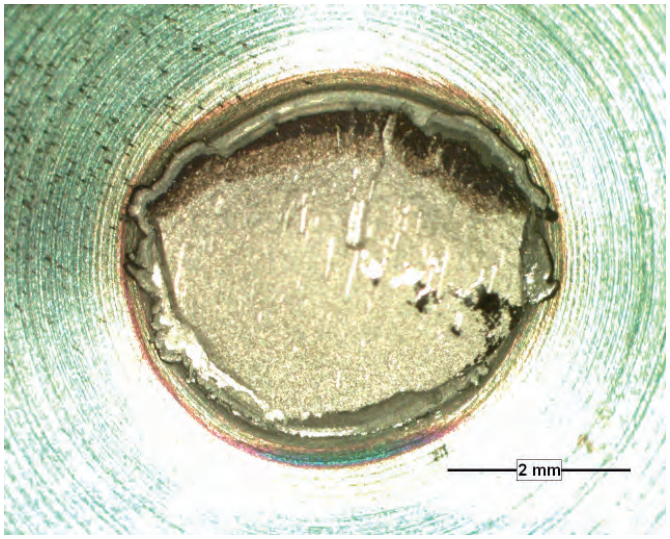

(a) Fracture surface on endcap side

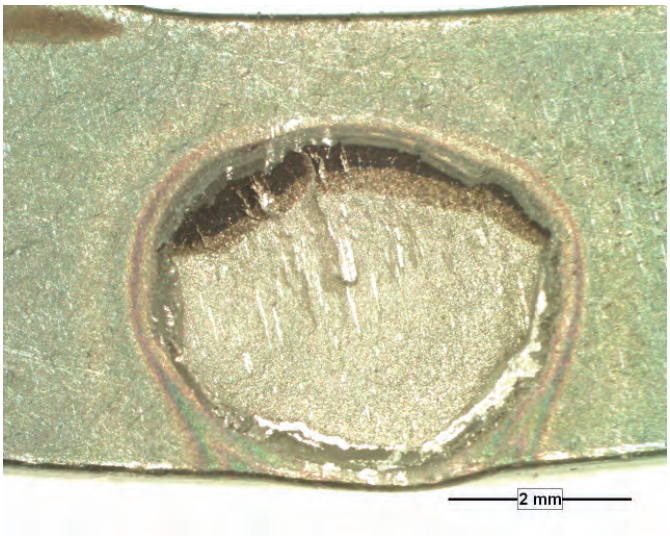

(b) Fracture surface on endplate side

Figure 26: Fracture surfaces of sample in Test 09-130 on GE 28-element bundle

Figure 26 shows the fracture surfaces on the endcap and endplate side. The two crack segments corresponding to the K_{IH} and DHCV test are clearly visible. The fracture surface is similar to that of Test 09-125 in which cracking appeared to have initiated near the top of weld. The weld had an elliptical shape and was skewed towards the OD side of the endplate. Figure 27 shows the dimensions of the weld measured from the fracture surfaces and a schematic diagram of the endplate and endcap notch constructed from the measured dimensions. The

profile and location of the weld with respect to the endplate are similar to that of the sample in Test 09-125.

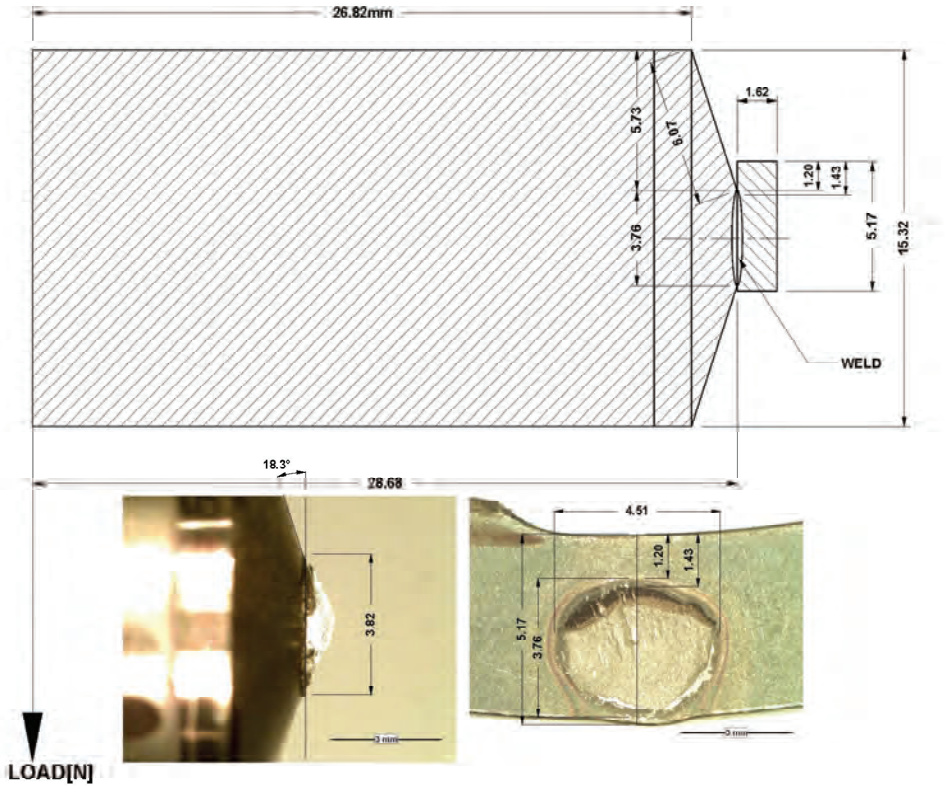

Figure 27: Dimensions of welds measured from fracture surfaces in Test 09-130 on GE 28 element bundle

Test 09-144: This test was performed on the endplate weld of element # 15 in DHC rig # 6 with the ID side of the endplate loaded under tension. The sample was subjected to both the K_{IH} and DHCV test procedures. The test record was similar to that of Test 09-123 and cracking was initiated at an applied load of 56 N.

Figure 28 shows the fracture surface on the endcap and endplate side which are similar to that of Tests 09-125 and 09-130. Cracking appeared to have initiated from the top of the weld. The

weld had an elliptical shape and skewed towards the OD side of the endplate. Figure 29 shows the dimensions of the weld measured from the fracture surfaces and a schematic diagram of the endplate and endcap notch constructed from the measured dimensions.

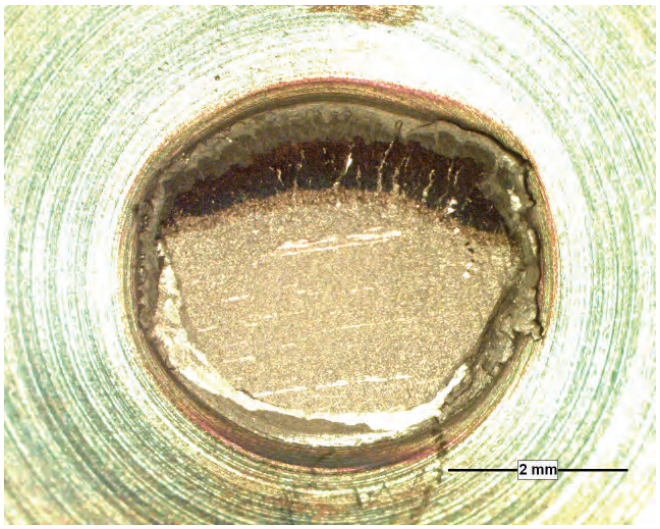

(a) Fracture surface on endcap side

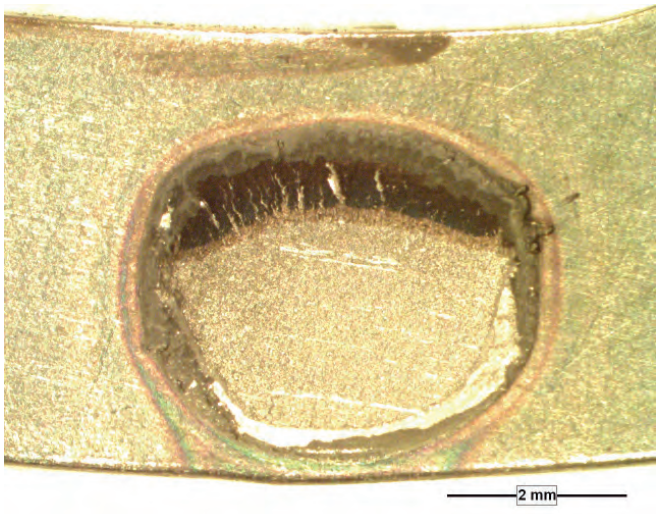

(b) Fracture surface on endplate side

Figure 28: Fracture surfaces of sample in Test 09-144 on GE 28-element bundle

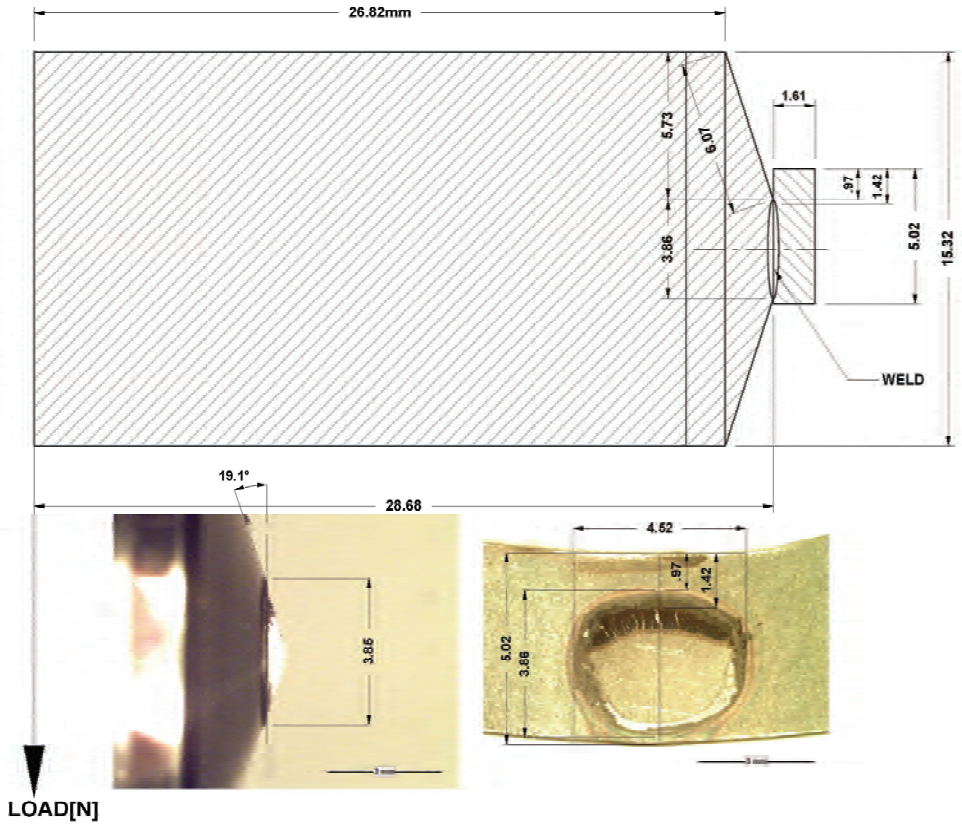

Figure 29: Dimensions of welds measured from fracture surfaces in Test 09-144 on GE 28-element bundle

Test 09-172: This test was performed on the endplate weld of element # 6 in DHC rig # 6 with the ID side of the endplate loaded under tension. The sample was subjected to both the K_{IH} and DHCV test procedures. The test record was similar to that of Test 09-123 and cracking was initiated at an applied load of 53 N.

Figure 30 shows the fracture surfaces on the endcap and endplate side. The two crack segments corresponding to the K_{IH} and DHCV test are visible. Cracking was initiated at the top of weld. The weld had an elliptical shape and was skewed towards the OD side of the endplate. Figure 31 shows the dimensions of the weld measured from the fracture surfaces and a schematic diagram of the endplate and endcap notch constructed from the measured dimensions.

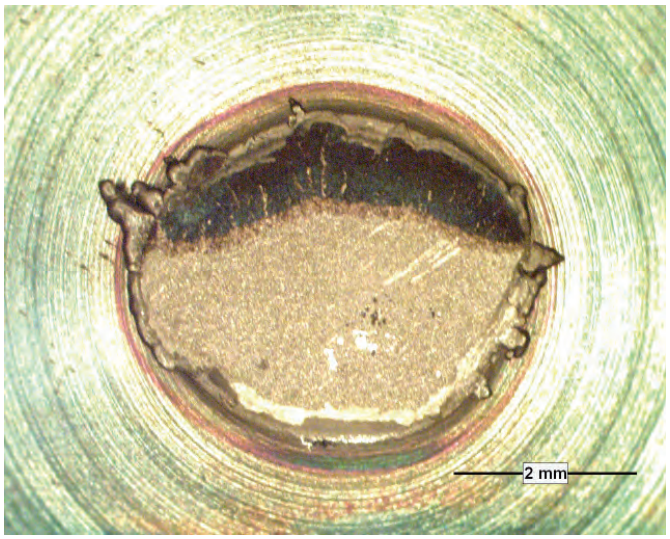

(a) Fracture surface on endcap side

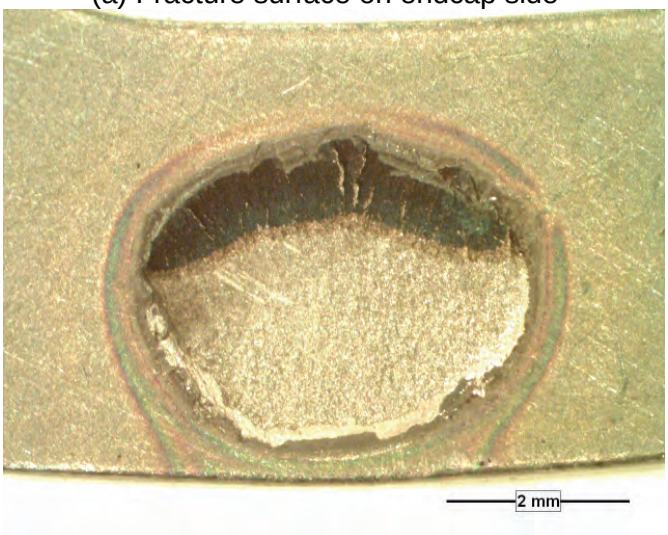

(b) Fracture surface on endplate side

Figure 30: Fracture surfaces of sample in Test 09-172 on GE 28-element bundle

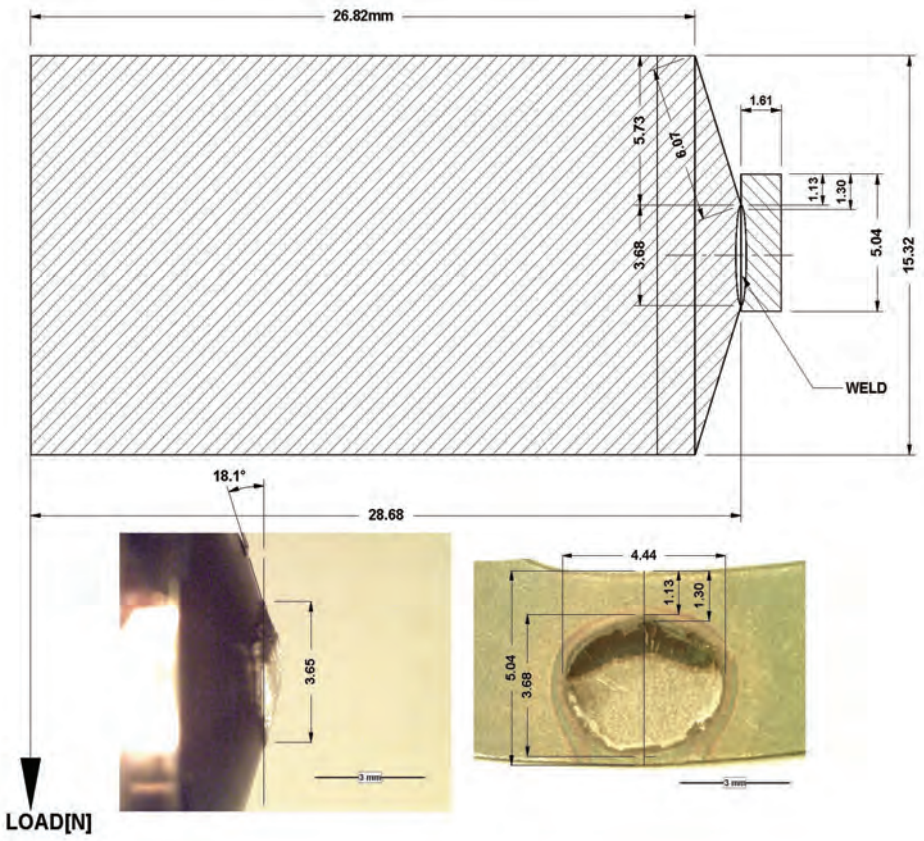

Figure 31: Dimensions of welds measured from fracture surfaces in Test 09-172 on GE 28 element bundle

Test 09-182: This test was performed on the endplate weld of element # 8 in DHC rig # 6 with the OD side of the endplate loaded under tension. The sample was subjected to both the K_{IH} and DHCV test procedures. Figure 32 shows the test record which indicates that cracking initiated at an applied load of 74 N, which is significantly higher than the tests with the sample loaded on the ID side.

Figure 33 shows the fracture surfaces on the endcap and endplate side. Unlike the tests with the samples loaded on the ID side, cracking appeared to have initiated near the 45° away from the top of the weld. The weld was skewed towards the OD side of the endplate. Figure 34 shows the dimensions of the weld measured from the fracture surfaces and a schematic diagram of the endplate and endcap notch constructed from the measured dimensions.

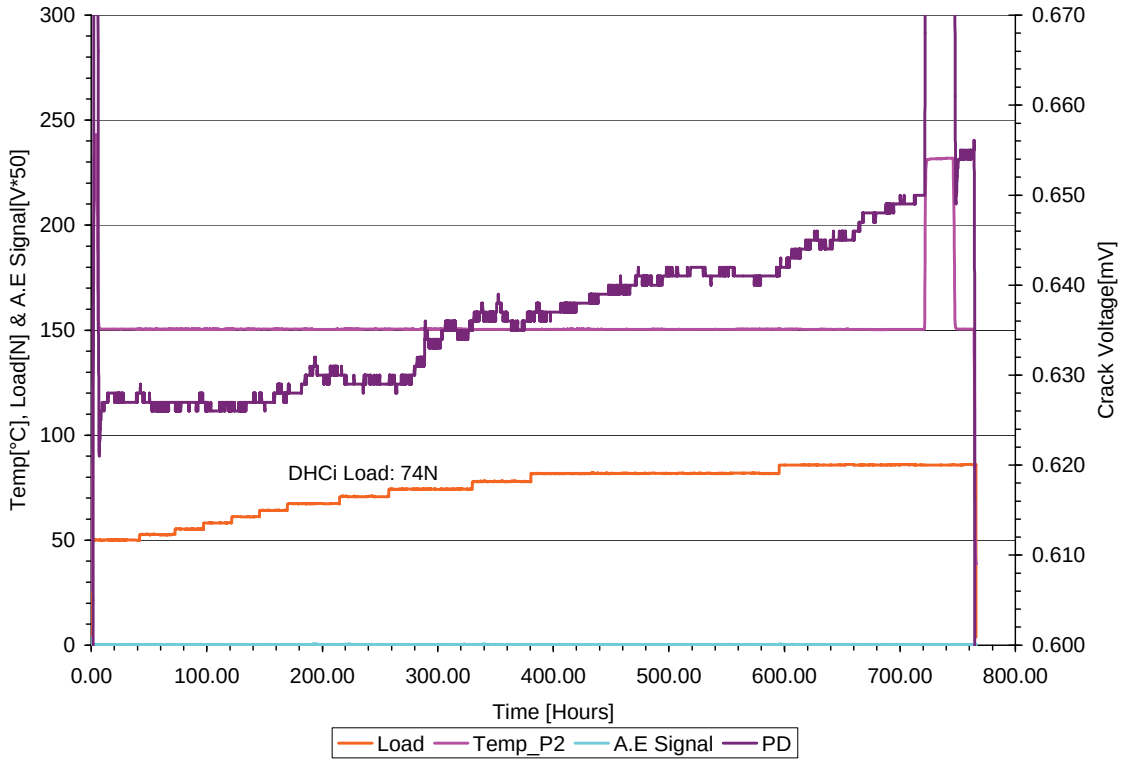

Figure 32: Record of K_{IH} and DHCV tests in Test 09-182 on element # 8 of the GE 28-element bundle; sample loaded on the OD side of the endplate

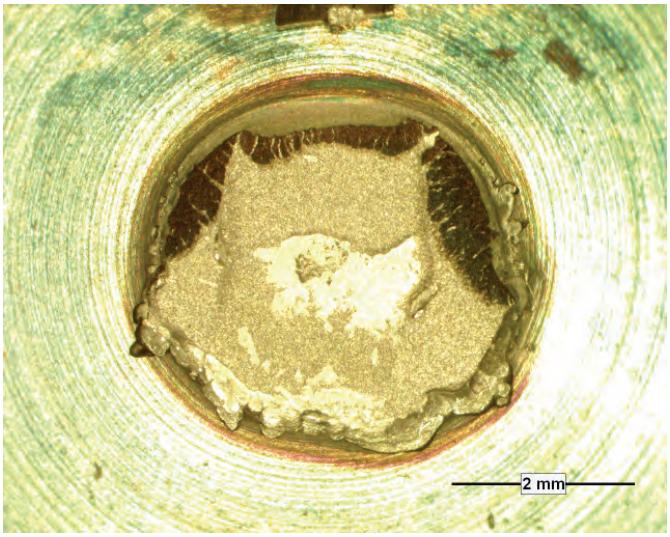

(a) Fracture surface on endcap side

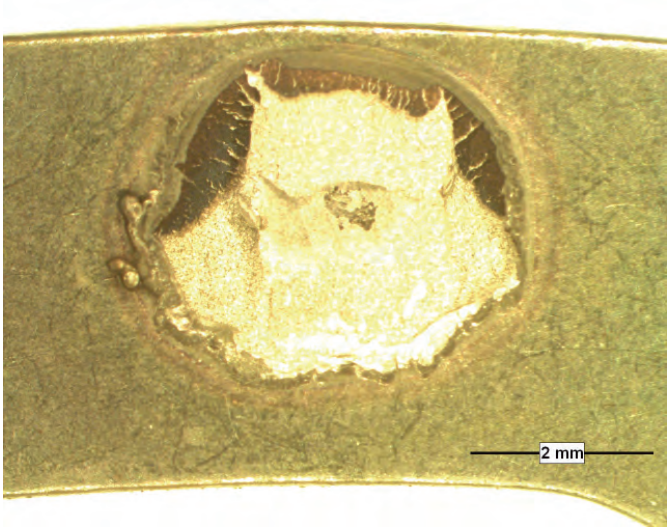

(b) Fracture surface on endplate side

Figure 33: Fracture surfaces of sample in Test 09-182 on GE 28-element bundle in which the OD side was loaded under tension

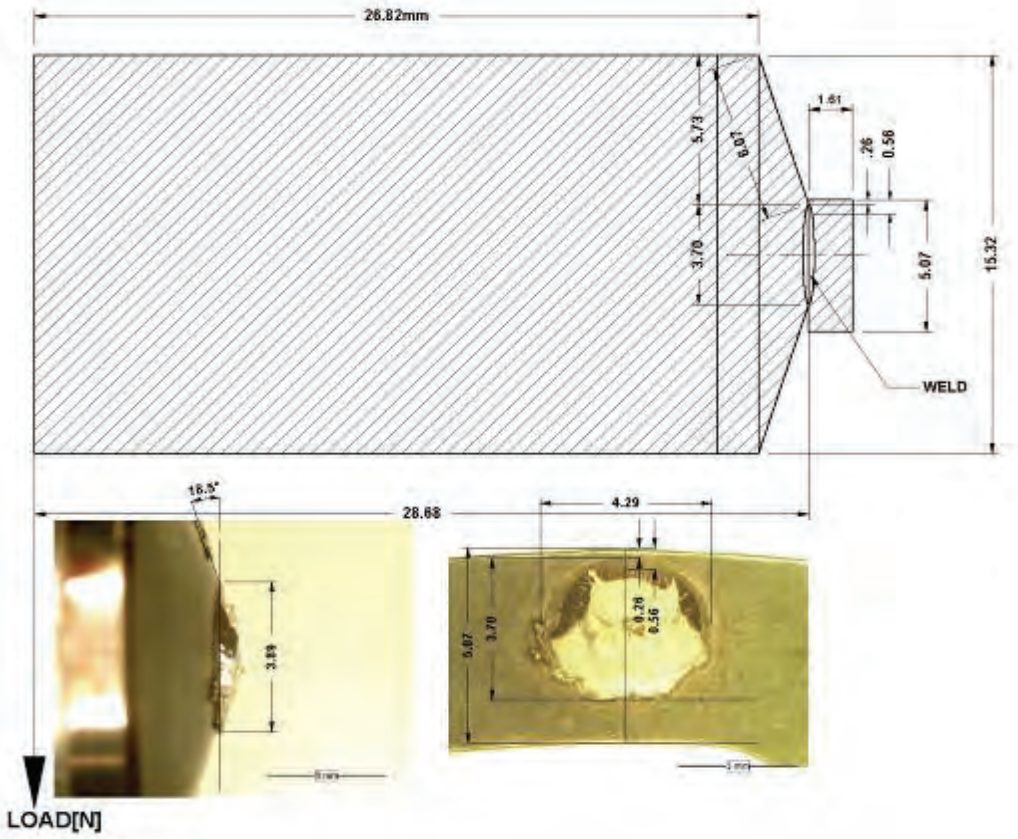

Figure 34: Dimensions of welds measured from fracture surfaces in Test 09-182 on GE 28 element bundle

3.3 CAMECO 37-ELEMENT BUNDLE

Five K_{IH} tests were performed in which the samples were loaded on the ID side of the endplate. A DHCV test was performed on one sample. No DHC test was performed with the sample loaded on the OD side of the weld. As will be seen from the test results described below and in Wasiluk (2011), no valid K_{IH} values could be obtained from two of the endplate welds. Results of the applied bending stresses and K_{IH} values for DHC initiation determined in Wasiluk (2011) are summarized in Table 5.

Test 09-135: This test was performed on the endplate weld of element # 6 in DHC rig # 6 in with the ID side of the endplate loaded under tension. Figure 35 shows the sample which was subjected to the K_{IH} test procedure only. Figure 36 shows the test record. No increase in potential drop was observed after the load was incrementally increased to 80 N. At this load level, significant vertical deflection of the sample was observed through the furnace window. Testing was terminated at this stage without the heat-tinting cycle.

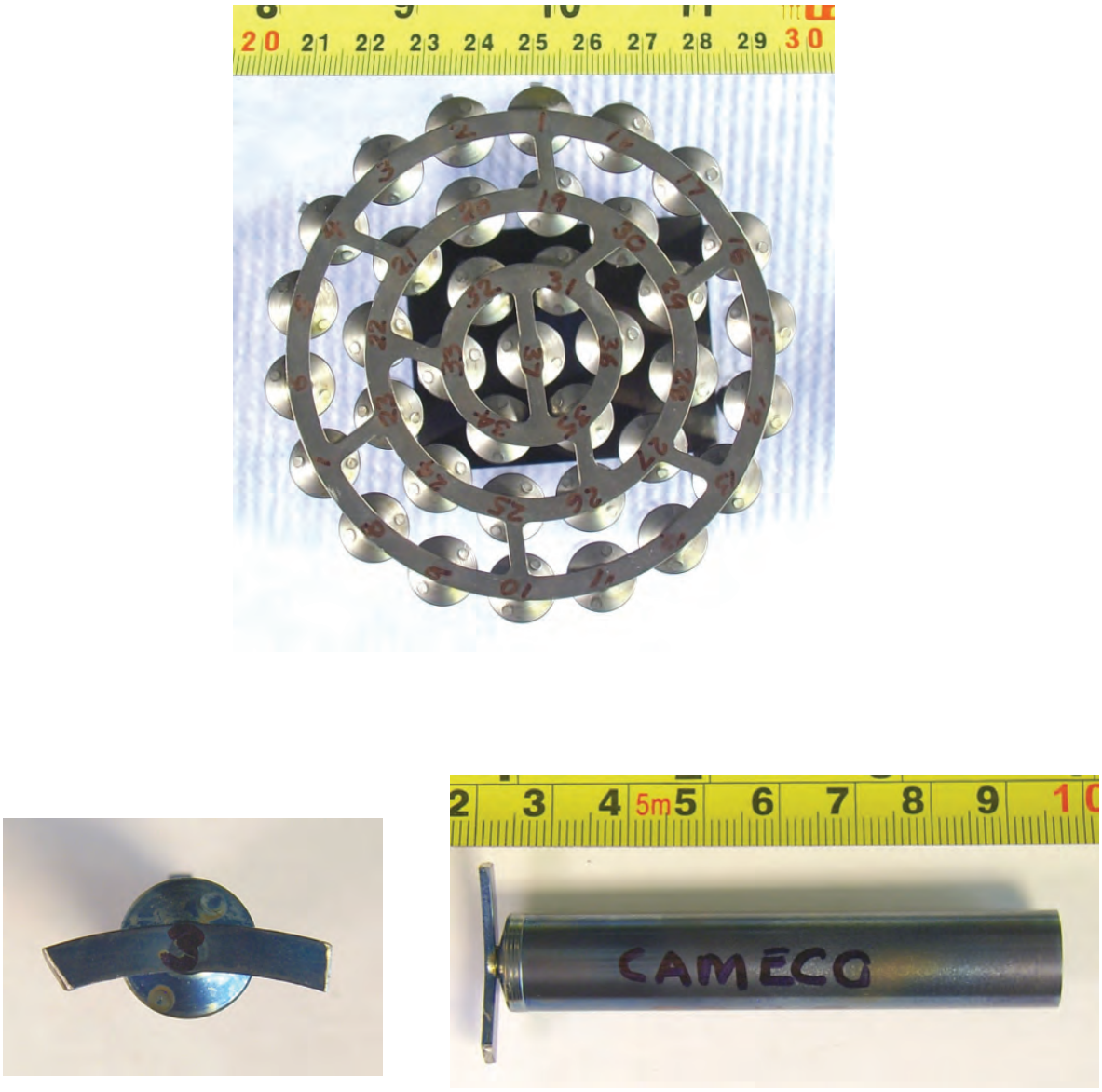

Figure 35: Sample for Test 09-135 from the CAMECO 37-element bundle

After the DHC test, the sample was examined metallographically to determine the notch profile and weld continuity. The sample was sectioned near the edge the weld (Figure 37a), mounted and then ground towards the weld. Figure 37b shows the section in the as-polished condition at about 1.7 mm from the mid-section of the weld. It should be noted that the notch at this plane

will appear deeper, as it is not at the mid-section of the weld. At higher magnification, a crack was observed at the ID side of the weld which grew at about 30° into the endplate side of the weld (Figure 37c). The sample was anodized which revealed the hydride layer on the sample surface (Figure 37d). At the higher magnification, the crack path appeared to be decorated with hydride particles. At this plane, the DHC crack was about 424 µm long. Upon further grinding to the mid-section of the weld, the crack disappeared as shown in Figure 38. The notch at the mid-section of the weld was relatively blunt and no weld discontinuity was observed.

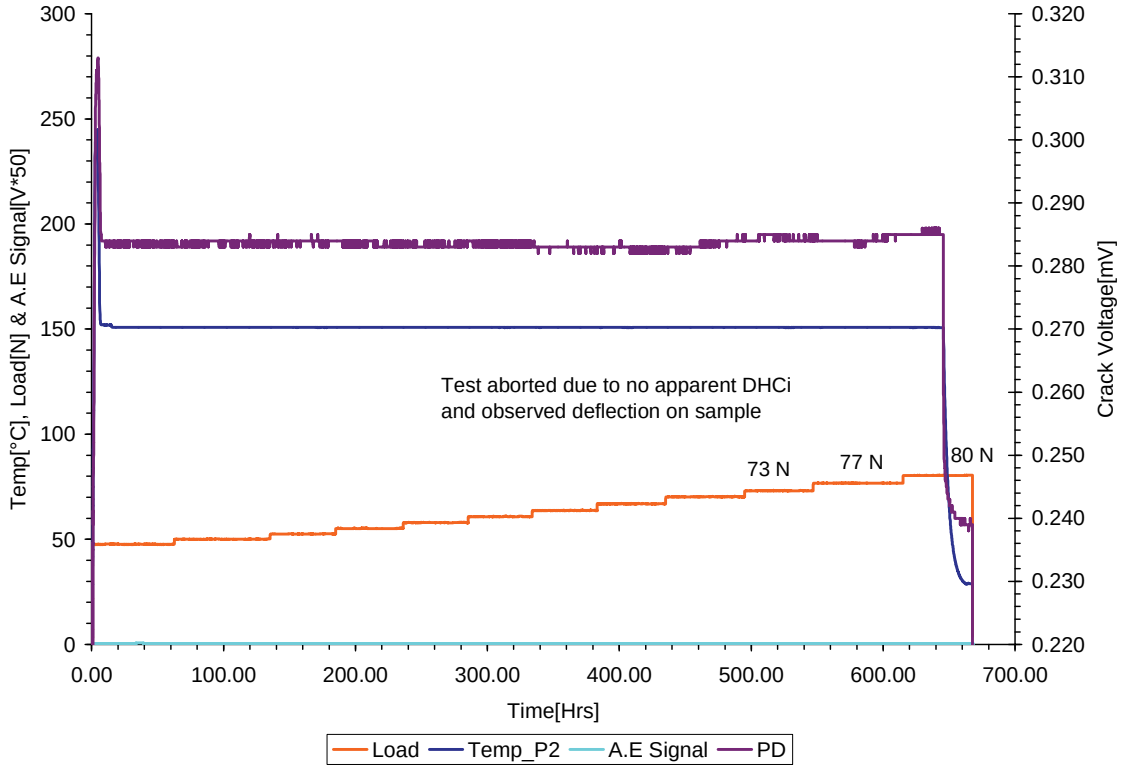

Figure 36: Records of Test 09-135 on element #3 of the CAMECO 37-element bundle

Based on the above observation, it is postulated that a DHC crack was initiated near the 45° location away from the top of the weld. The DHC crack did not extend to the top of the weld. This could be the reason that cracking was not detected by the potential drop as the probes were placed across the top of the weld. As cracking was not detected during the DHC test, it is not feasible to determine the crack initiation load from the potential drop record. However, one can calculate the cracking time using an estimated DHCV and a maximum crack length.

Assuming a maximum crack length of 424 µm and a DHCV of 8×10^{-10} m/sec (see other CAMECO test summarized in Table 5), it is estimated that the cracking time was about 147 hours. This suggests that cracking was initiated at 73 N according to the record shown in Figure 36. As fractographic examination was not performed to characterize the dimensions of the weld geometry and depth of weld discontinuity, it was not feasible to calculate the K_{IH} value of this endplate weld.

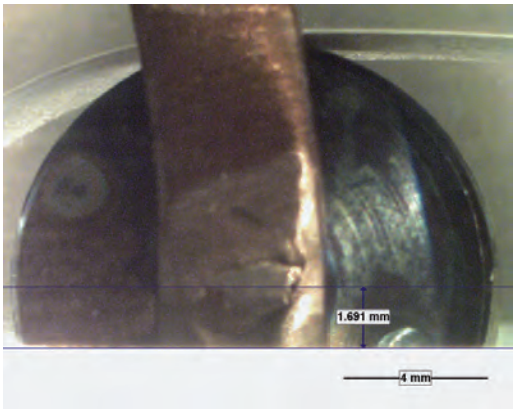

(a) Top view of sample

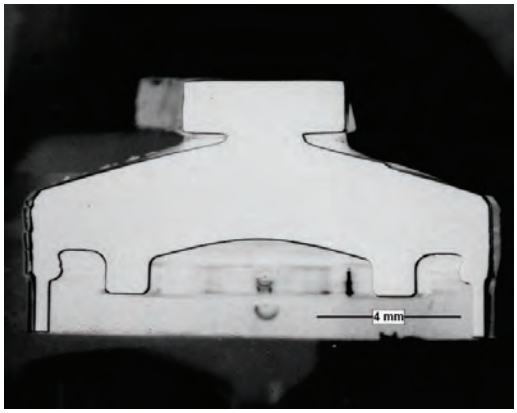

(b) As-polished; 1.7 mm from centre of weld

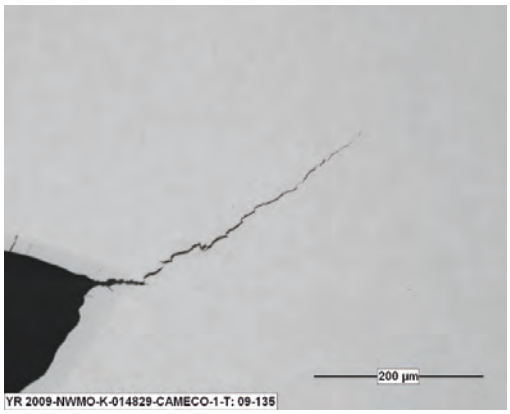

(c) As-polished; higher magnification showing the crack on the ID side of endplate

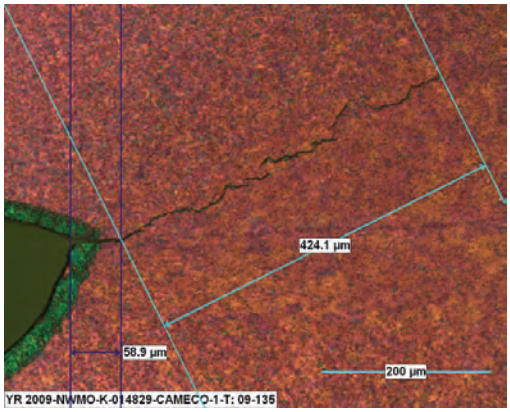

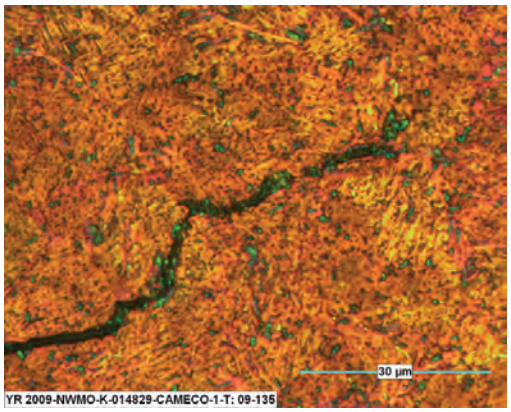

(d) Anodized; showing hydride layer on surface and hydride particles along the crack

Figure 37: DHC crack shown in metallographic section about 1.7 mm from mid-section of weld of sample from Test 09-135

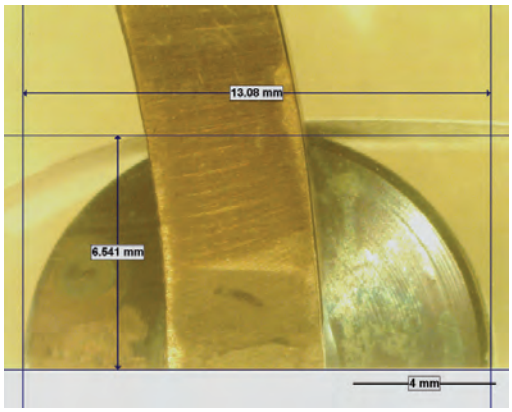

(a) Top view of sample

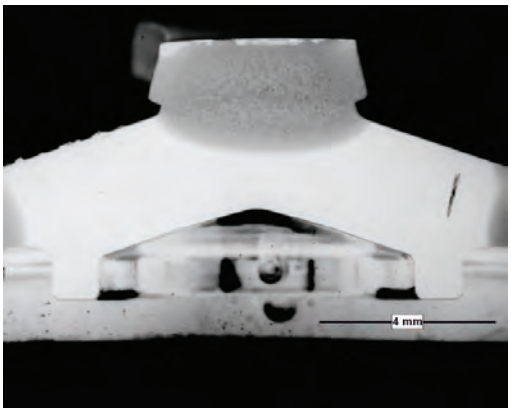

(b) As-polished; centre of weld

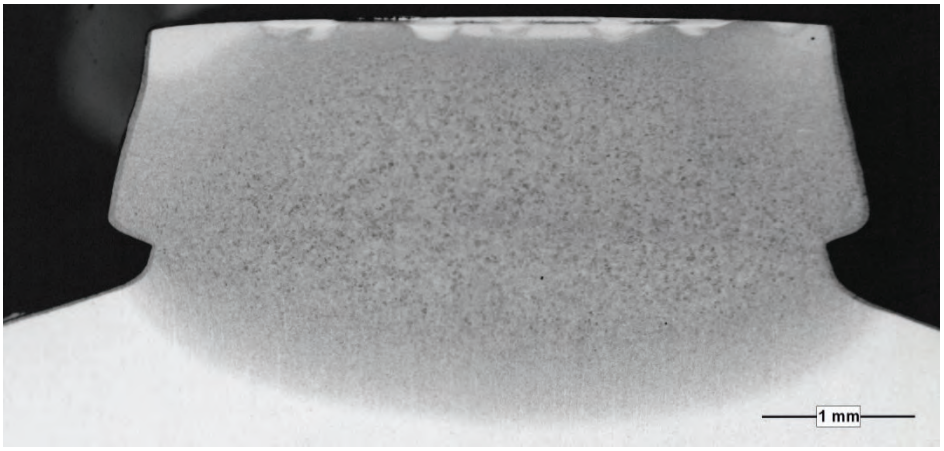

(c) Anodized showing the weld and heat-affected-zone

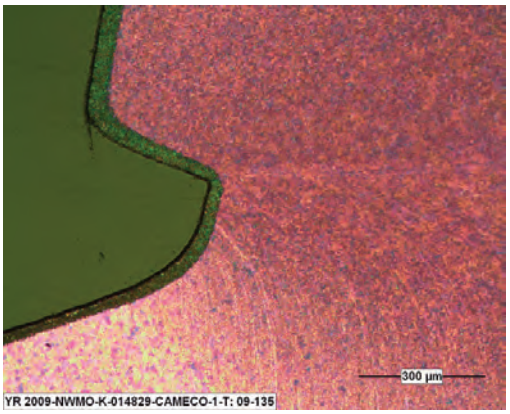

(d) Anodized, ID side, no DHC crack

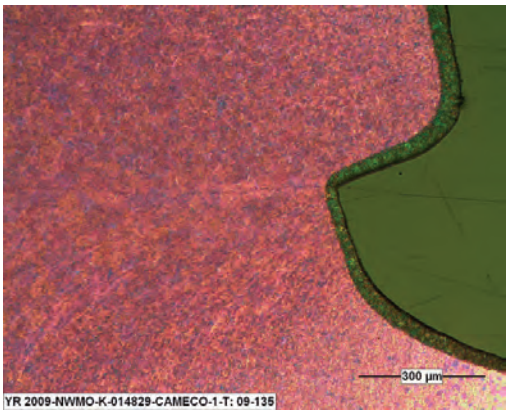

(e) Anodized, OD side

Figure 38: Metallographic section near centre of weld of sample from Test 09-135

Test 09-186: The test was performed on the endplate weld of element # 18 in DHC rig # 4 with the ID side of the endplate loaded under tension. The sample was subjected to the K_{IH} test procedure only. This test was performed at the same time as 09-135 in a separate loading rig. Figure 39 shows the test record in which no cracking was detected at a final load of 89 N. At this load, there was a large deflection of the sample and testing was terminated without the heat-tinting thermal cycle

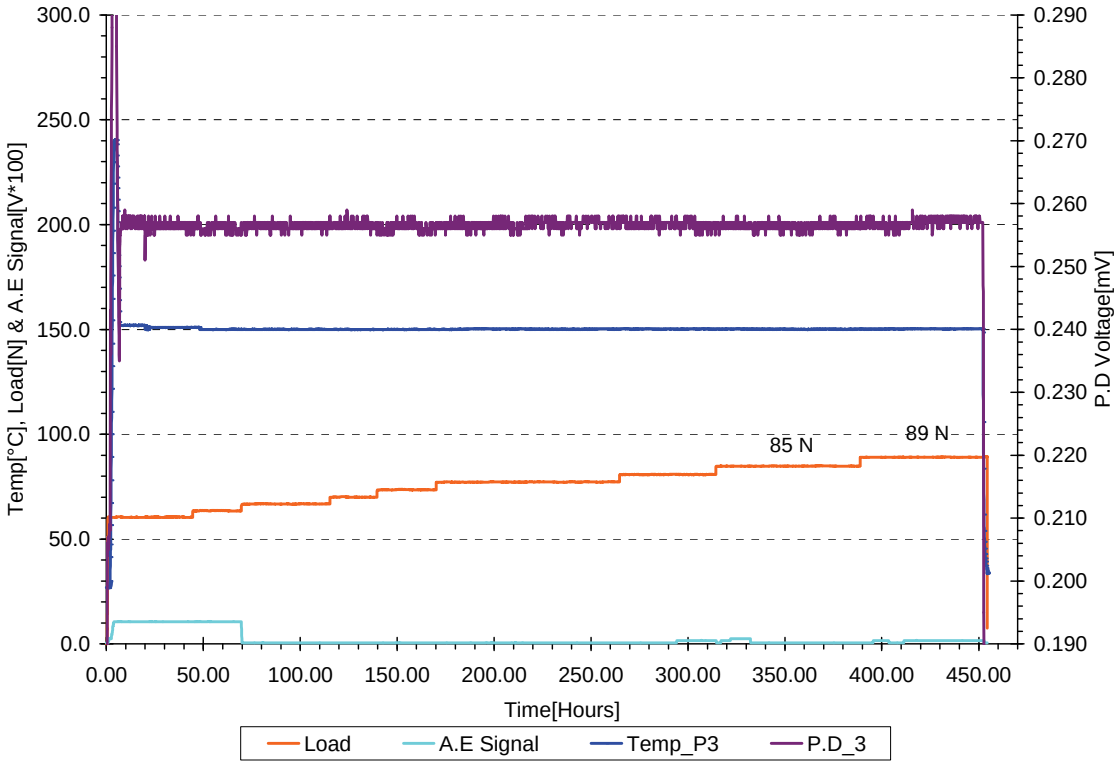

Figure 39: Record of K_{IH} test in Test 09-186 on element #18 of the CAMECO 37-element bundle; sample loaded on ID side of endplate

After the DHC test, the sample was peeled open and a small crack with a thin surface oxide was observed at a location about 45° from the top (Figure 40). The crack length was estimated to be about 0.25 mm. Using an estimated DHCV of 8×10^{-10} m/sec, the estimated cracking time was about 88 hours which suggested that cracking was initiated at a load of 85 N, according to test record shown in Figure 39.

Figure 41 shows the dimensions of the weld measured from the fracture surfaces and a schematic diagram of the endplate and endcap notch constructed from the measured dimensions. The K_{IH} value for this weld was calculated in Wasiluk (2011) and the result is shown in Table 5.

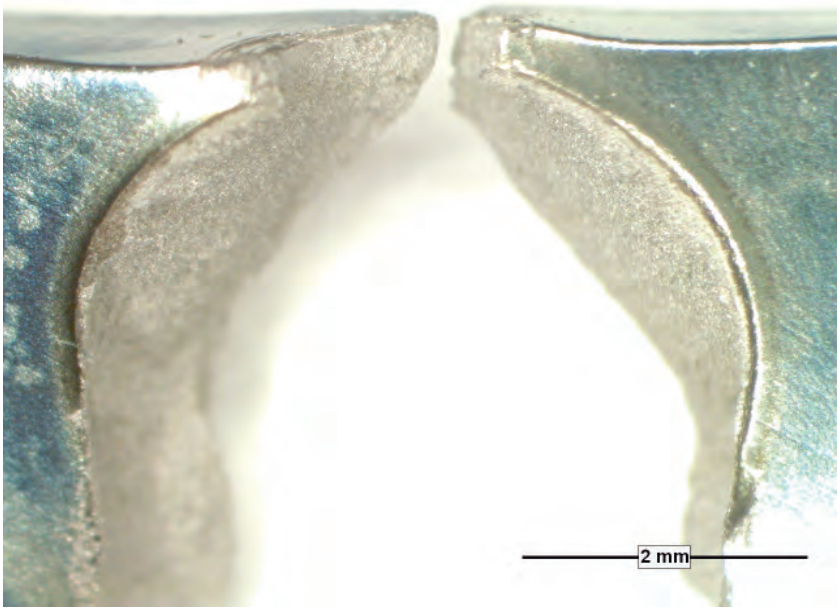

Figure 40: A small crack with thin oxide was observed on the sample of Test 09-186

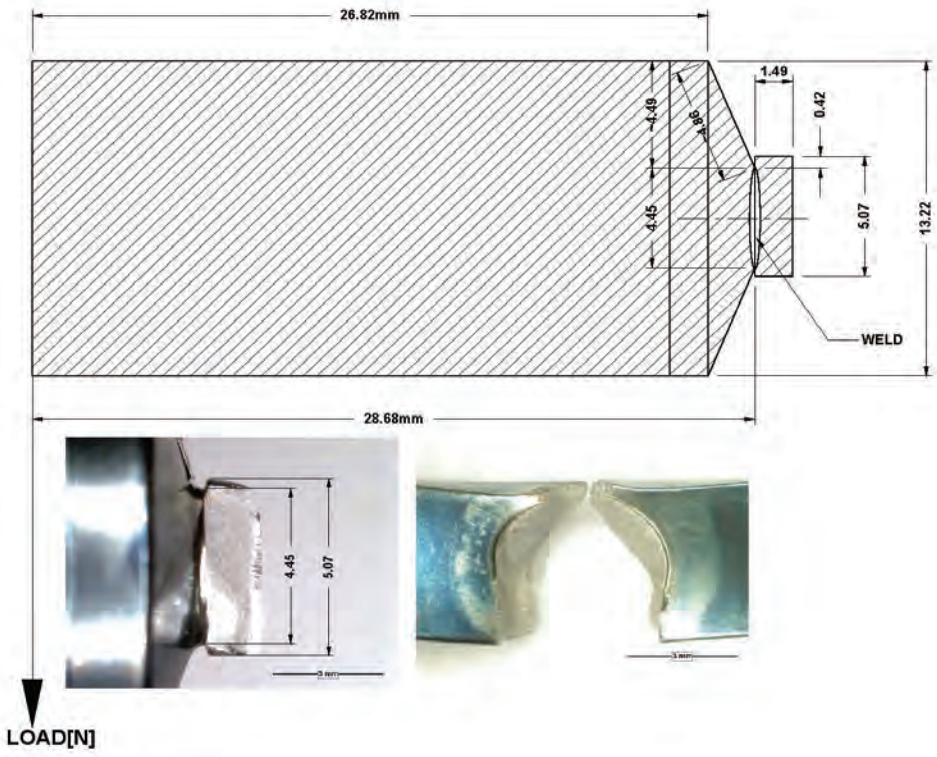

Figure 41: Dimensions of welds measured from fracture surfaces in Test 09-186 on CAMECO 37-element bundle

Test 09-204: The test was performed on the endplate weld of element # 5 in DHC rig # 4 with the ID side of the endplate loaded under tension. The sample was subjected to both K_{IH} and DHCV test procedures. In this test, three sets of potential drop probes were used for crack detection: at the top of the weld and at the two locations about 45° away from the top of the weld (Figure 42). Figure 43 shows the test record of Test 09-204 which indicates that cracking appears to initiate at both 45° locations at an applied load of 80 N.

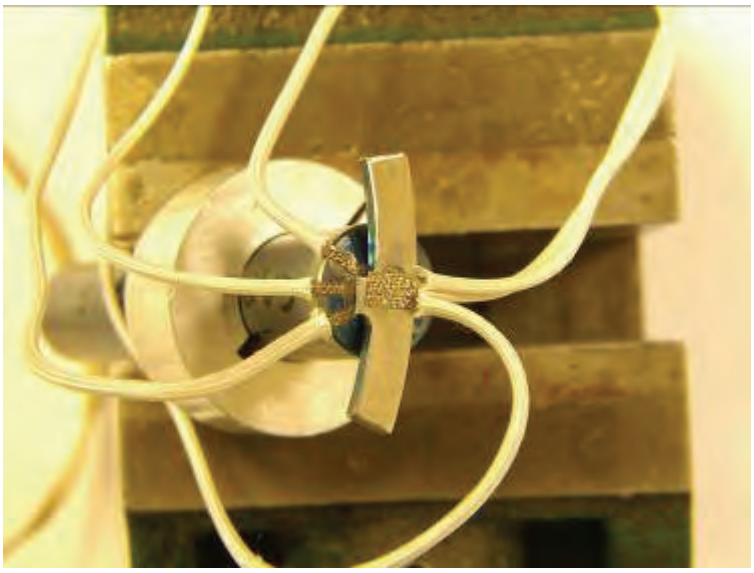

Figure 42: Three sets of potential drop leads were placed on the sample of some of the tests performed on CAMECO 37-element fuel bundle

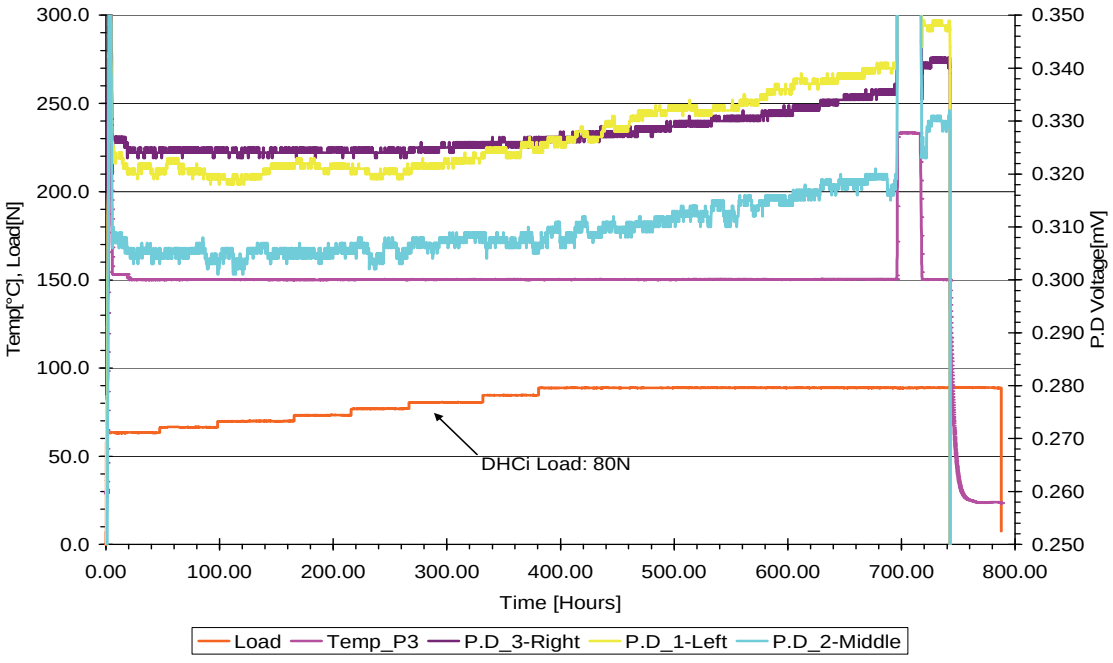

Figure 43: Record of KIH and DHCV tests in Test 09-204 on element # 5 of the CAMECO 37-element bundle; sample loaded on the ID side of endplate

Figure 44 shows the fracture surfaces of the DHC cracks on the endcap and endplate side. The two crack segments corresponding to the K_{IH} and DHCV are visible in which cracking appeared to be initiated at the two locations about 45° from the top of the weld. Figure 45 shows the dimensions of the weld measured from the fracture surfaces and a schematic diagram of the endplate and endcap notch constructed from the measured dimensions. The K_{IH} value for this weld was calculated in Wasiluk (2011) and the result is shown in Table 5.

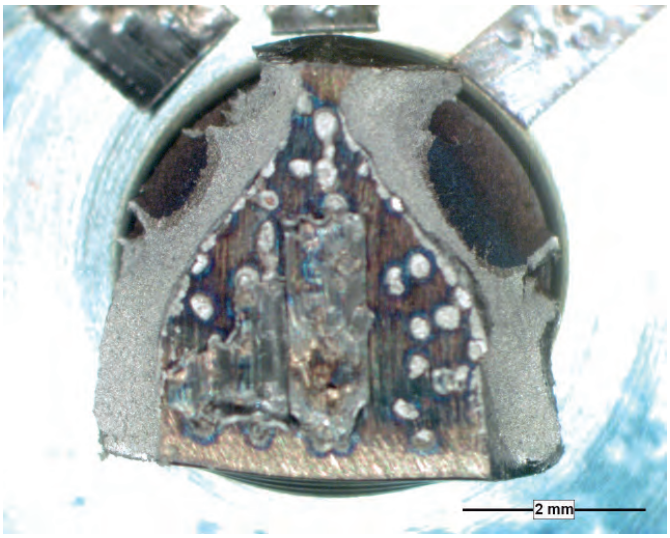

(a) Fracture surface on endcap side

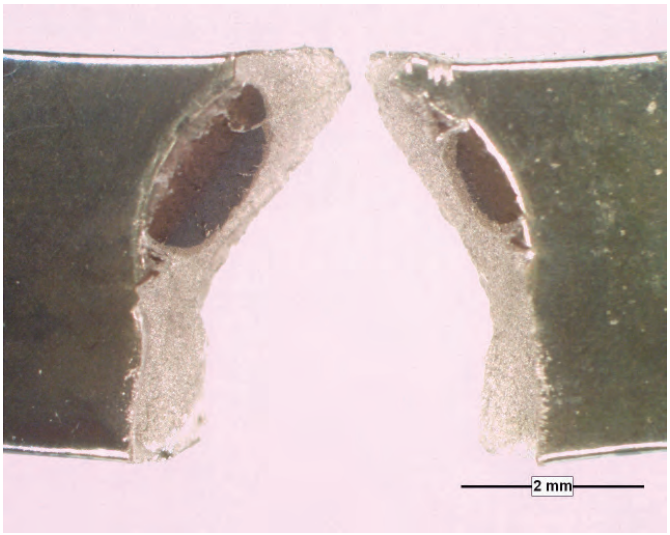

(b) Fracture surface on endplate side

Figure 44: Fracture surfaces of sample in Test 09-204 of CAMECO 37-element bundle

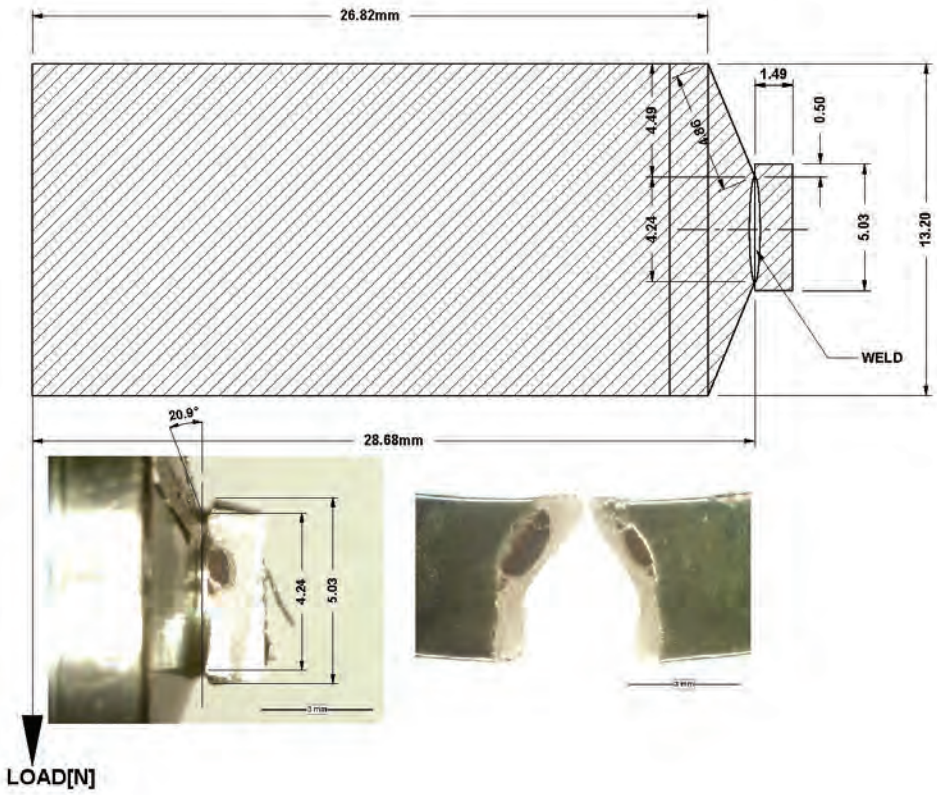

Figure 45: Dimensions of welds measured from fracture surfaces in Test 09-204

Test 09-208: The test was performed on the endplate weld of element # 16 in DHC rig # 6 with the ID side of the endplate loaded under tension. As shown in Figure 46, the endplate of this sample contained a portion of the radial brace material. The sample was subjected to the K_{IH} test procedure only. Similar to the set-up in Test 09-204, three sets of potential drop probes were used for crack detection. However, the potential drop probe at the top of the weld was detached during testing and no data was obtained from that probe. Figure 47 shows the test record of Test 09-208 which indicates that cracking appears to initiate at both 45° locations at an applied load of 80 N.

Figure 48 shows the fracture surfaces of the DHC cracks on the endcap and endplate side. Cracking appears to be initiated at the two locations about 45° from the top of the weld. Figure 49 shows the dimensions of the weld measured from the fracture surfaces and a schematic diagram of the endplate and endcap notch constructed from the measured dimensions. As discussed in Wasiluk (2011), the K_{IH} value of this endplate could not be determined using the current finite-element model as a result of the presence of the brace material in the endplate.

Figure 46: Sample for Test 09_208 from the CAMECO 37-element bundle; Element 16 is at one of locations with the radial brace between the outer and intermediate rings

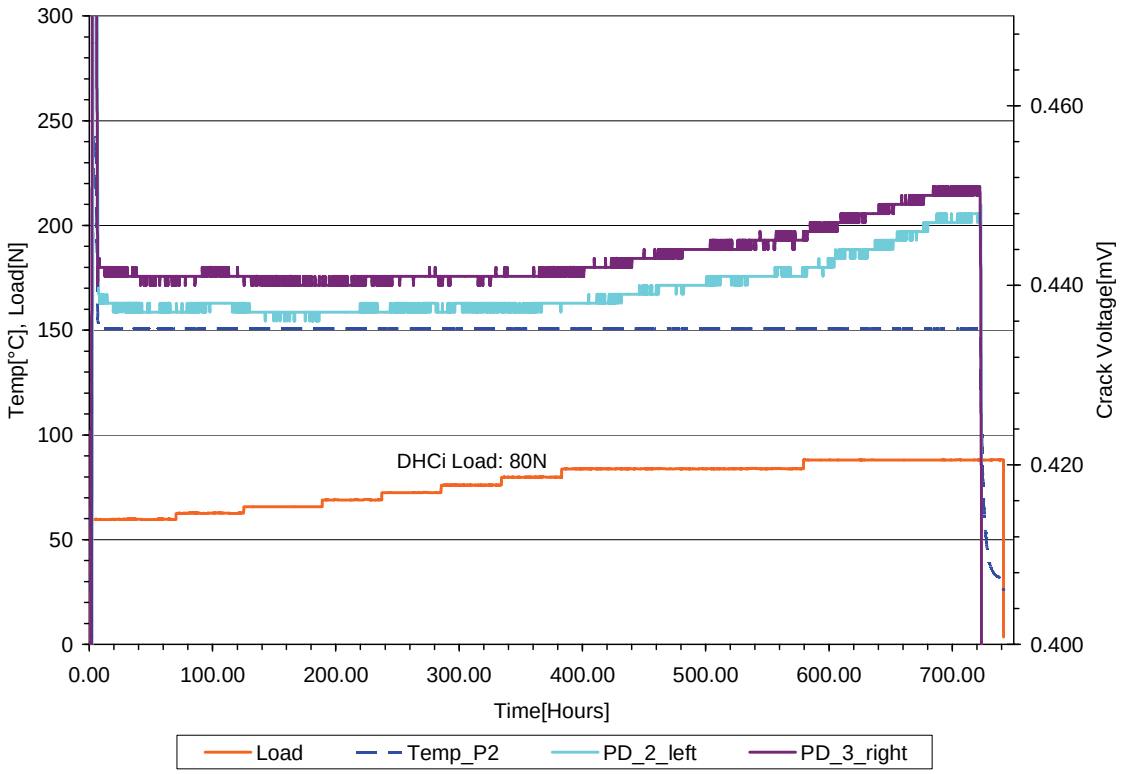

Figure 47: Record of K_{IH} test in Test 09-208 on element # 16 of the CAMECO 37-element bundle

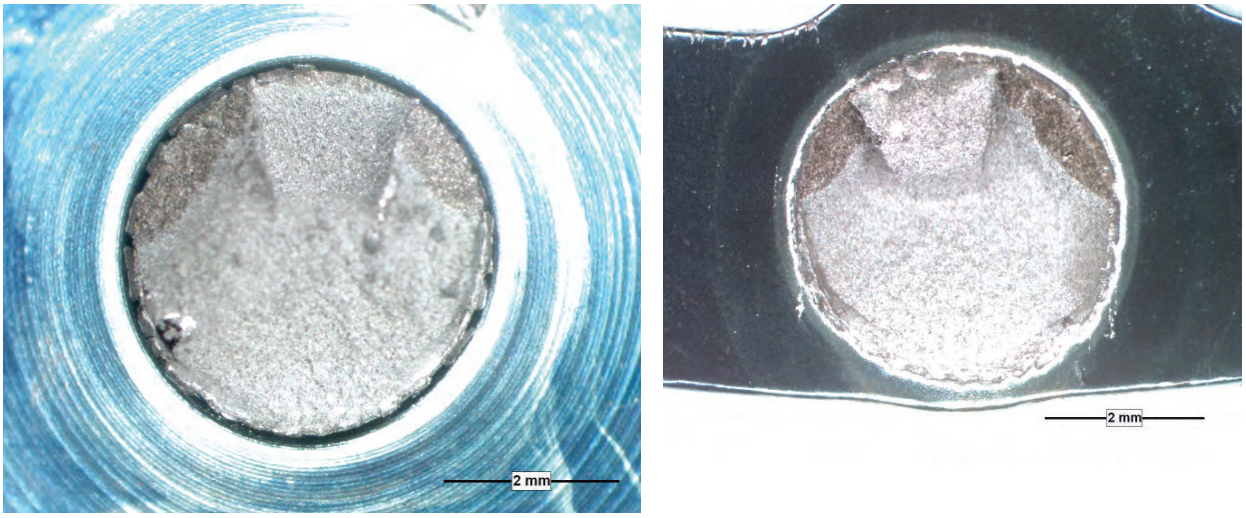

(a) Fracture surface on endcap side (b) Fracture surface on endplate side

Figure 48: Fracture surfaces of sample in Test 09_208 on CAMECO 37-element bundle

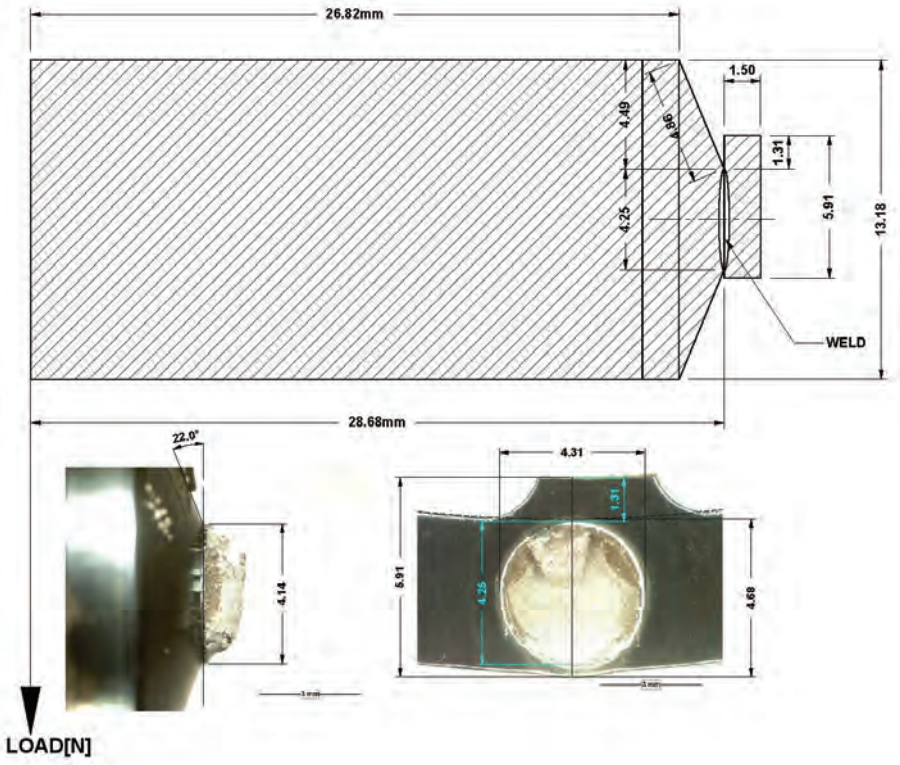

Figure 49: Dimensions of welds measured from fracture surfaces in 09_208

Test 10-16: The test was performed on the endplate weld of element # 9 in DHC rig # 4 with the ID side of the endplate loaded under tension. The sample was subjected to the K_{IH} test procedure only. Three sets of potential drop probes were used for crack detection. Figure 50 shows the test record of Test 10-16 in which no clear indication of cracking was detected by the potential drop technique when the test was terminated at an applied load 93 N.

After the DHC test, the sample was peeled open and a small crack with a thin surface oxide was observed at a location about 45° from the top (Figure 51). The maximum crack length was measured to be about 0.31 mm. Using an estimated DHCV of 8×10^{-10} m/sec, the estimated cracking time was about 108 hours which suggested that cracking was initiated at the final load of 93 N according to the test record shown in Figure 50.

Figure 52 shows the dimensions of the weld measured from the fracture surfaces and a schematic diagram of the endplate and endcap notch constructed from the measured dimensions. The K_{IH} value for this weld was calculated in Wasiluk (2011) reference [4] and the result is shown in Table 5.

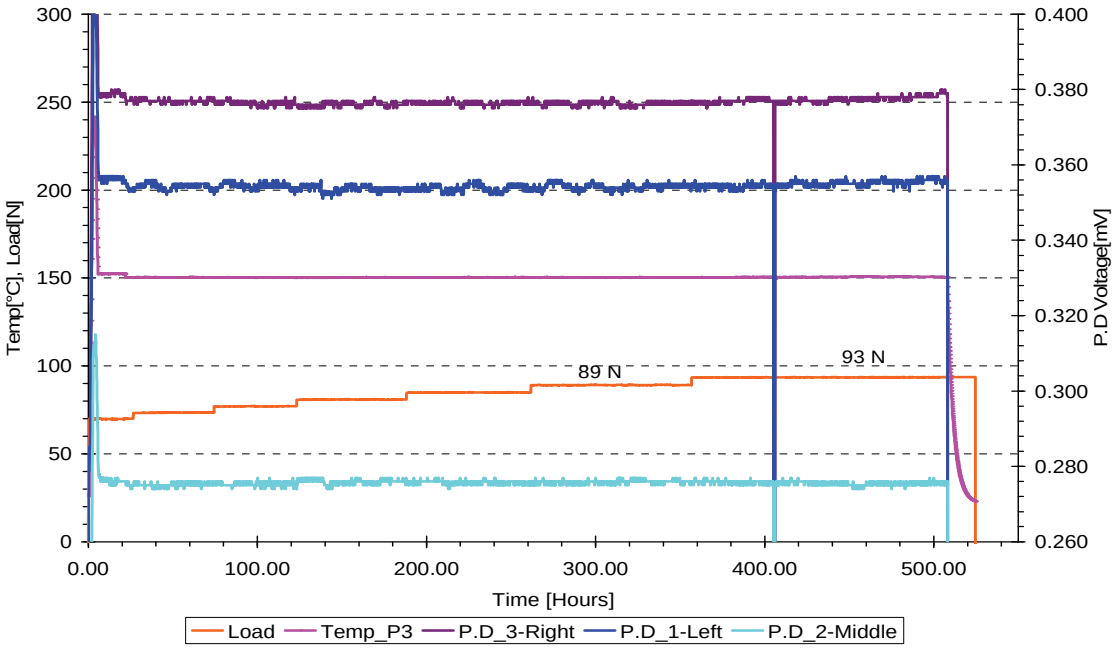

Figure 50: Record of K_{IH} test in Test 10-16 of the CAMECO 37-element bundle

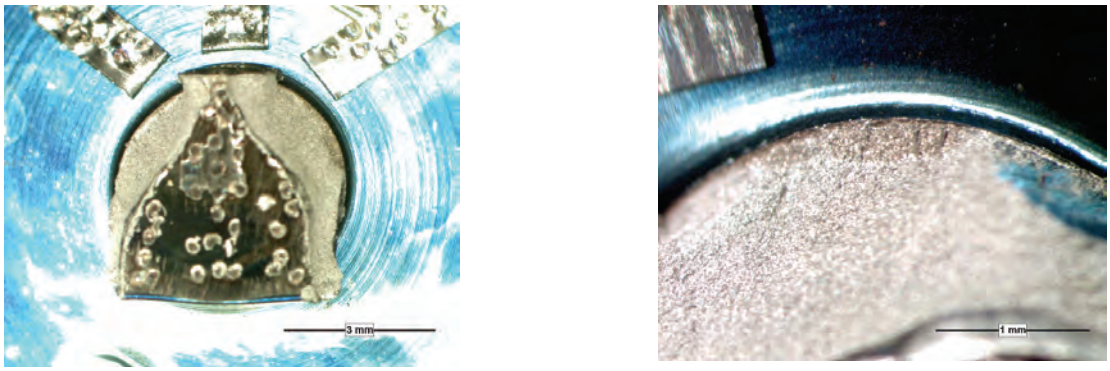

(a) Fracture surface on endcap side at two magnifications

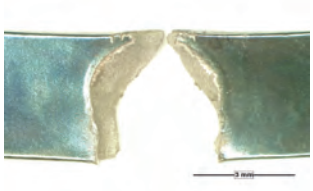

(b) Fracture surface on endplate side

Figure 51: Fracture surfaces of sample in Test 10-16 on CAMECO 37-element bundle

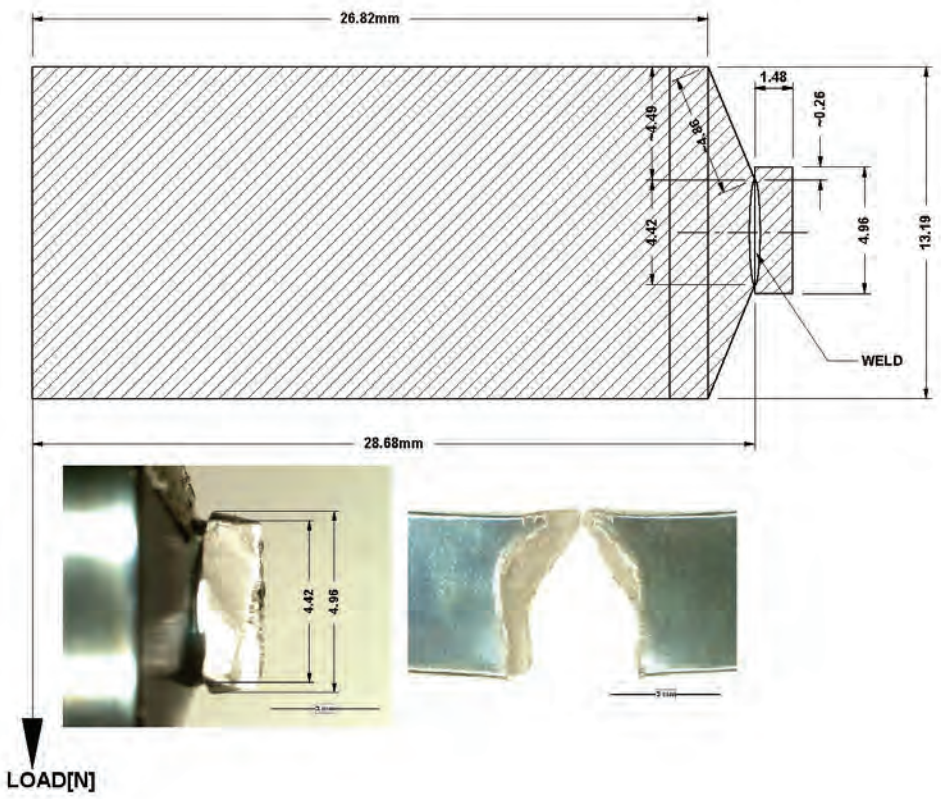

Figure 52: Dimensions of welds measured from fracture surfaces in Test 10-16

3.4 OTHER OBSERVATIONS

In Section 3.3, it was mentioned that significant sample deflection was observed towards the end of the K_{IH} tests when the samples were loaded to a relatively high load. This is illustrated in Figure 53 showing the sample deflection at various stages in Test 09-135 (CAMECO sample loaded from the ID side in Test Rig # 6). Figure 53a is the reference position when the sample was installed in the loading rig without applied load. The end of the sample was deflected for about 2.5 mm when a load of 48 N was applied at room temperature before enclosing the loading assembly in the furnace (Figure 53b). If the load was removed at this stage, the sample would spring back to the reference position. The deflection increased to about 6 mm when the applied load was raised to 80 N at the end of the K_{IH} test (Figure 53c). The 6 mm deflection was measured at room temperature after the furnace was removed from the loading assembly. When the load was removed at this stage, there was a permanent deflection of about 3 mm from the reference position (Figure 53d).

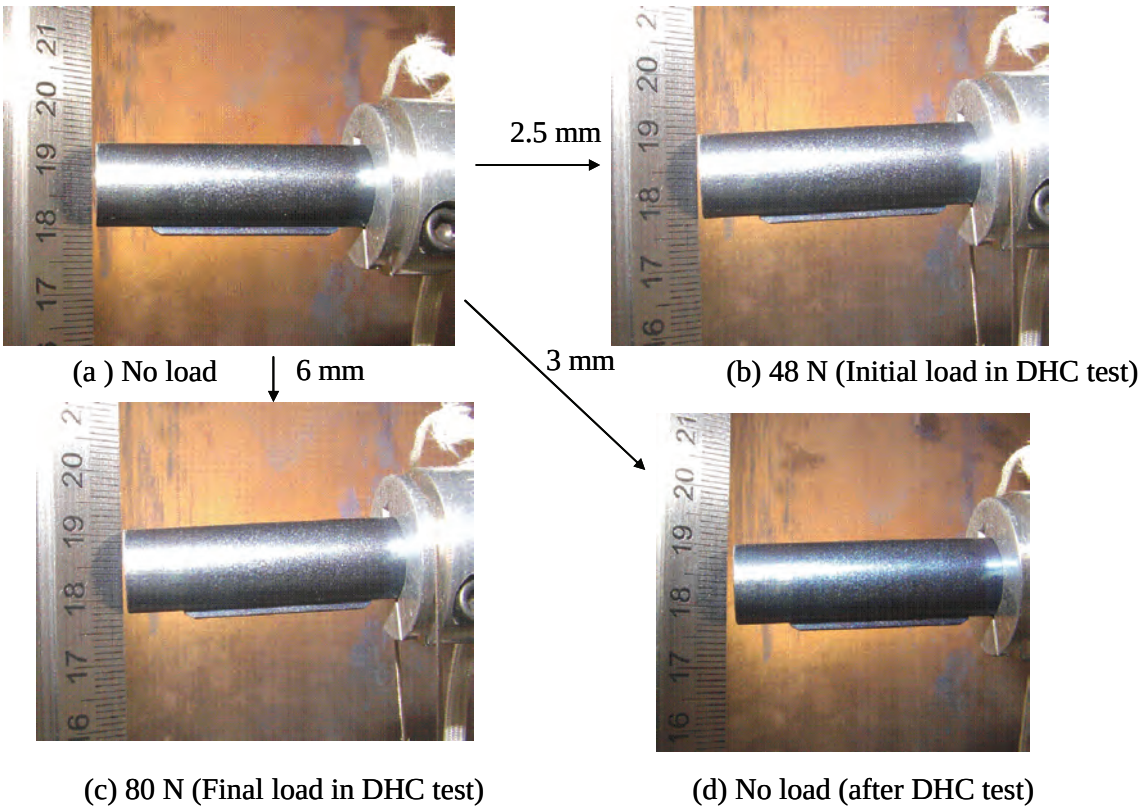

Figure 53: Deflection of sample in Test 09-135 (CAMECO bundle, DHC ring #6) at different loading stages

4. DISCUSSION

4.1 APPLIED BENDING STRESSES AND K_{IH} VALUES FOR DHC INITIATION

Figure 54 compares the applied bending stresses for DHC initiation from the endplate welds of the three fuel bundles tested in the current program and the GE 37-element bundle tested in Shek and Wasiluk (2009). The applied bending stresses to initiate DHC cracking were lower for the GE 37-element bundle tested in Shek and Wasiluk (2009). For the three bundles tested in the current program, it appears that the GE 37-element bundle welds had the highest bending stresses for DHC initiation, followed by the CAMECO 37-element bundle. The GE 28-element bundle welds had the lowest bending stresses for DHC initiation. For the GE 28-element bundle, the bending stress required for DHC initiation was higher when the weld was loaded on the OD side of the endplate than when it was loaded from the ID side, due to the difference in notch depth as a result of the weld skewed towards the OD side. The variability in applied bending stress for DHC initiation from the endplate welds of the different fuel bundles is likely due to both differences in weld geometry and material properties.

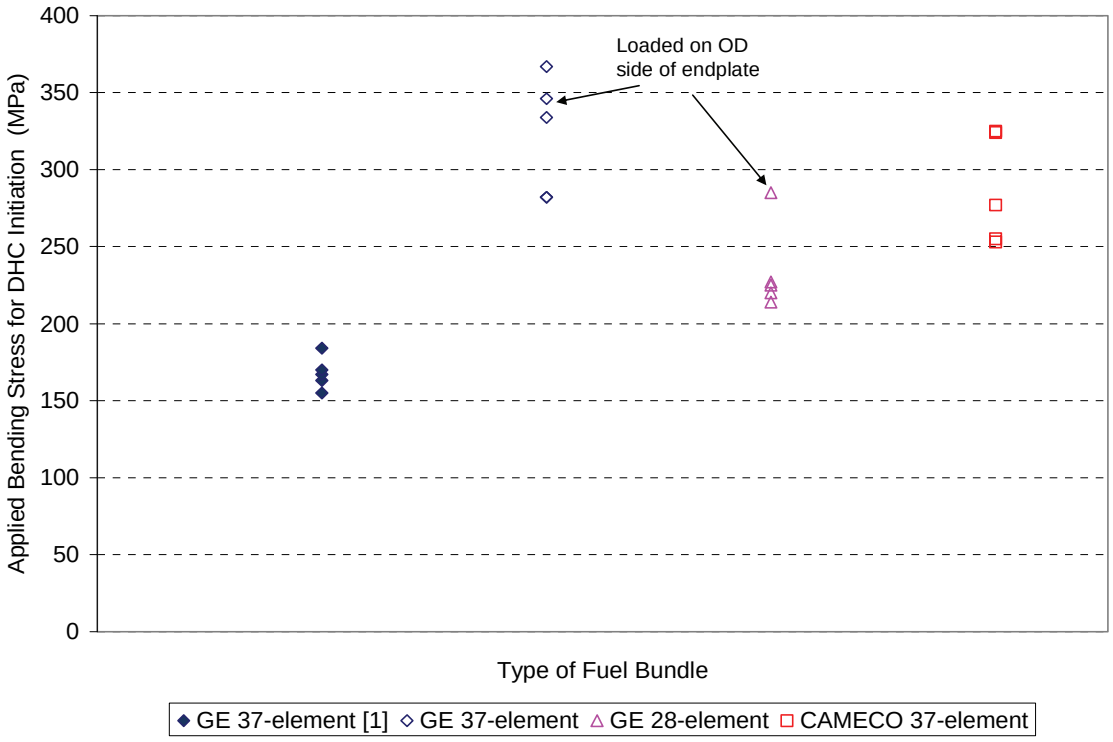

Figure 54: Comparison of applied bending stress for DHC initiation of endplate welds from different fuel bundles

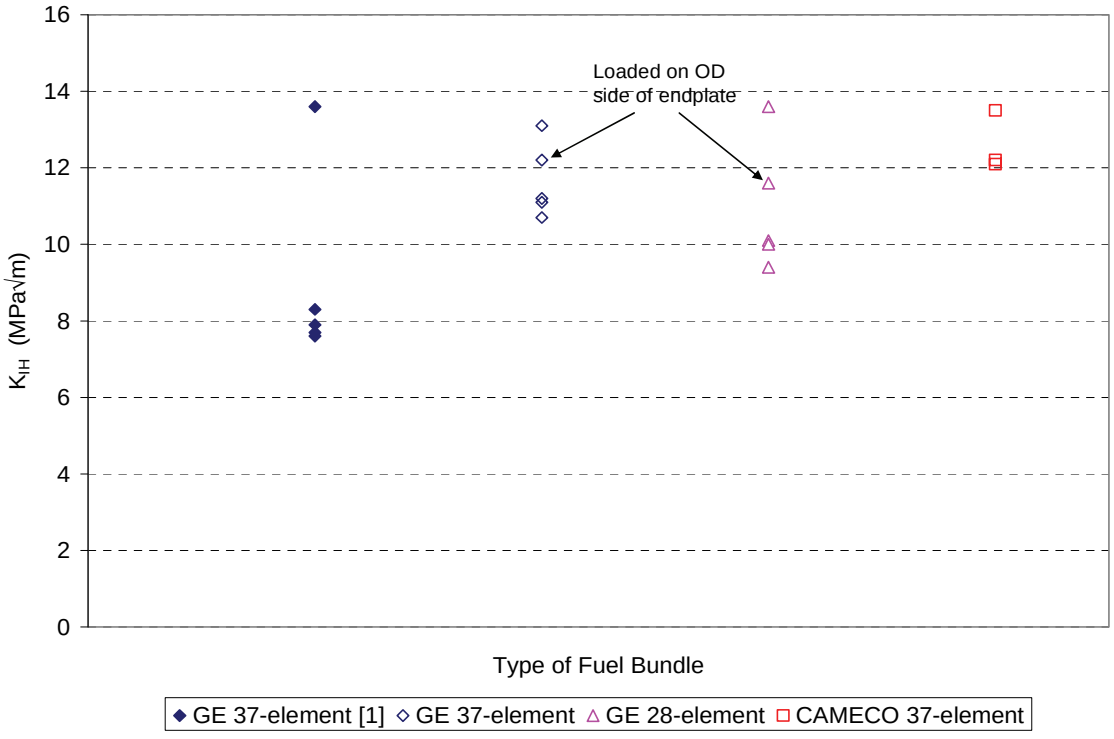

Figure 55: Comparison of K_{IH} values of endplate welds from different fuel bundles

Figure 55 compares the K_{IH} values for DHC initiation from the endplate welds of the three fuel bundles tested in the current program and the GE 37-element bundle tested in Shek and Wasiluk (2009). It appears that there were no large differences in K_{IH} values among the endplate welds of the three bundles tested in the current program. Furthermore, there was no large difference in K_{IH} values between the welds loaded on the ID and OD side of the endplate, within the scatter of the data. For the endplate welds of the GE 37-element bundle tested in Shek and Wasiluk (2009), four out of the five data appear to have lower K_{IH} values than that of the three bundles tested in the current program.

4.2 DHC VELOCITY

Figure 56 compares the DHCV at 150°C from the endplate welds of the GE 37-element bundle tested in reference [1] and the endplate welds of the three bundles tested in the current program. Only the two DHCV data from the outer element welds from Shek and Wasiluk (2009) are used for comparison. Within the scatter of the limited data, it appears that there are no large differences in DHCV of the endplate welds among the three bundles tested in the current year. The DHCV data from the GE 37-element bundle in Shek and Wasiluk (2009) are higher than those from the current test program.

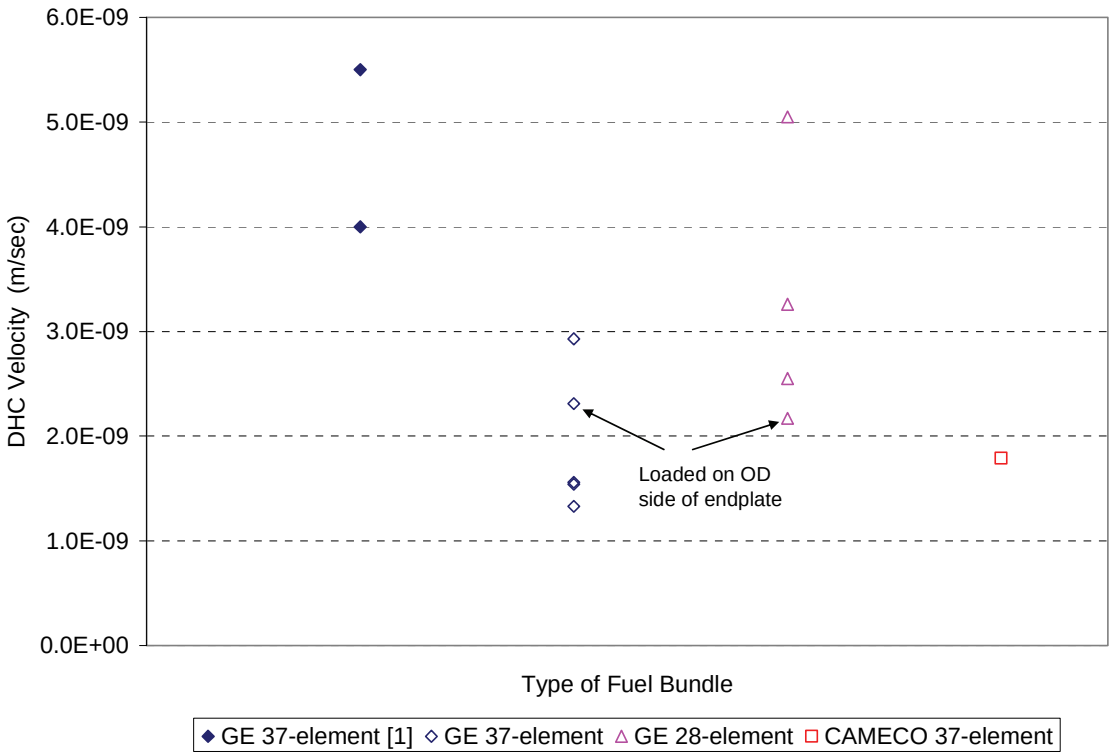

Figure 56: Comparison of DHCV at 150°C of endplate welds from different fuel bundles

5. CONCLUSIONS

The following observations and conclusions can be made from the tests performed on the GE 37-element, GE 28 element and CAMECO 37-element bundles in the current program and the tests performed on the GE 37-element bundle in Shek and Wasiluk (2009):

(1) There was variability in weld geometry such as the profile of the notch formed between the endplate and endcap, the weld discontinuity and weld area among the GE 37-element, GE 28-element and the CAMECO 37-element fuel bundles. In terms of the weld geometry, the endplate welds of the CAMECO 37-element bundle appear to be the least susceptible to DHC as the notch root radius was blunter and the weld discontinuity was either non-existent or small. There was also difference in the location of the welds with respect to the width of the endplate. The welds of the GE 28-element and CAMECO 37-element bundles were more skewed towards the OD side of the endplate than the welds of the GE 37-element bundle.

(2) The DHC cracks did not necessarily initiate at the top of the welds with respect to the loading orientation. The DHC cracks of the GE 37-element bundle and the CAMECO fuel bundles appear to have initiated at the location about 45° deviated from the top of the weld. However, most of the cracks of the GE 28-element bundle were initiated from the top of the weld, similar to that observed in the GE 37-element bundle tested in Shek and Wasiluk (2009).

(3) Among the three bundles tested in the current program, the applied bending stresses for DHC initiation from the endplate welds were highest for the GE 37-element bundle, followed by the CAMECO 37-element bundle and then the GE 28-element bundle. However, the bending stresses for DHC initiation from these three bundles were higher than that of the GE 37-element bundle tested in Shek and Wasiluk (2009). The limited data indicated that the applied bending stress for DHC initiation was higher when the weld was loaded on the OD side of the endplate than loaded from the ID side.

(4) The K_{IH} values of the endplate welds of the three fuel bundles tested in the current program were similar and appear to be higher than that of the GE 37-element bundle tested in Shek and Wasiluk (2009). Based on the limited data, there was no significant difference in K_{IH} values whether the weld was loaded from the ID side or OD side of the endplate.

(5) There was no large difference in DHCV at 150°C among the welds of the three bundles tested in the current program. The DHCV appear to be lower that of the GE 37-element bundle tested in Shek and Wasiluk (2009).

ACKNOWLEDGEMENTS

This work was funded by NWMO. Mr. H. Seahra of Kinectrics provided the technical support for the DHC tests and post-test examination.

REFERENCES

Kearns, J.J. 1967. Terminal Solid Solubility and Partitioning of Hydrogen in the Alpha Phase of Zirconium, Zircaloy-2 and Zircaloy-4. Journal of Nuclear Materials, Vol. 22, pp. 292-303.

Shek, G.K. and B.S. Wasiluk. 2009. Development of Delayed Hydride Cracking Test Apparatus and Commissioning Tests for CANDU Fuel Bundle Assembly Welds. Nuclear Waste Management Organization. NWMO TR-2009-08.

Shek, G.K., B. S. Wasiluk, T. Lampman and J. Freire-Canosa. 2008. Testing the Susceptibility of CANDU Fuel Bundle Endcap/Endplate Welds to Delayed Hydride Cracking, 10th CNS International Conference on CANDU Fuel, October 5-8.

Wasiluk, B.S. 2011. The Effect of CANDU Fuel Bundle Endplate/Endcap Weld Morphology on Computed Stress Intensity Factors at the Welds. Nuclear Waste Management Organization. NWMO TR-2011-03.